

# Performance-dependent changes in monkey prefrontal cortex during short-term memory

Dissertation

zur Erlangung des Doktorgrades  
der Naturwissenschaften

vorgelegt beim Fachbereich Physik  
der Johann Wolfgang Goethe–Universität  
in Frankfurt am Main

von

Wei Wu  
aus Hebei (China)

Frankfurt am Main 2008

(D30)

vom Fachbereich Physik der Johann Wolfgang Goethe–Universität als Dissertation angenommen.

Dekan: Prof. Dr. Dirk-Hermann Rischke

Gutachter: Dr. Gordon Pipa, Prof. Dr. Wolf Singer, Prof. Dr. Jochen Trisch

# Zusammenfassung

Zwecks Untersuchung der neuronalen Verarbeitung im Kurzzeit-Gedächtnis nahmen wir im präfrontalen Kortex zweier Affen, welche eine visuelle Kurzzeitgedächtnisaufgabe lösten (0,5 Sekunden Aufnahme, 3 Sekunden Verzögerung, 2 Sekunden Test), gleichzeitig LFPs und Spikes auf. Wir untersuchten das aufgenommene Signal auf der Grundlage der Richtig-Falsch-Antworten der Affen nach einem zugrunde liegenden Mechanismus im Kurzzeit-Gedächtnis des Affen.

Zunächst analysierten wir verhaltensabhängige Veränderungen der Kopplung zwischen simultan abgeleiteten lokalen Feld-Potentialen (,LFPs') und der Aktivität einzelner (,Single-Unit-Aktivität') oder kleiner Gruppen von Neuronen (,Multi-Unit-Aktivität'), um die neuronalen Mechanismen im Kurzzeitgedächtnis bei der Informations-Kodierung und -Aufrechterhaltung über verschiedene räumliche Skalen hinweg zu untersuchen.

Informationsverarbeitungs-Abläufe beinhalten neuronale Kreisläufe auf verschiedenen räumlichen Skalen. Ihr Beitrag kann mittels der Analyse verschiedener Signale wie von einzelnen oder wenigen einzelnen Neuronen (,Mikroskopisch'), kleineren Populationen von Neuronen (,Mesoskopisch'), und Massen-Signalen wie LFP (,Makroskopisch') studiert werden.

Interaktionen zwischen diesen verschiedenen Ebenen sind von besonderem Interesse, wenn die Informationsverarbeitung Verhaltensübergängen oder Zustandsänderungen unterliegt, selbst wenn diese klein sind. Wir studierten

diese Interaktionen und testeten, ob eine Änderung der Beziehung zwischen der synaptischen Aktivität, gemessen durch das mesoskopische Signal des LFP und der Spike-Aktivität kleiner neuronaler Populationen im lateralen präfrontalen Kortex, wenn aufgenommene Information gespeichert und beim Vergleichen mit neuem Sinneseindruck wieder abgerufen werden muss, die Grundlage zur Wahl der passenden Verhaltensantwort ist.

Um die Interaktionen zwischen der lokalen mikroskopischen und dem mesoskopischen LFP zu charakterisieren, nutzten wir die Kohärenz zwischen der Spike-Aktivität und dem lokalen Feld-Potential (,Spike-Feld-Kohärenz') und analysierten, ob und auf welche Weise sich diese Spike-Feld-Kohärenz verhaltensabhängig während einer visuellen Kurzzeitgedächtnisaufgabe verändert. Dazu verglichen wir die Aktivität, die während Versuchsdurchgängen mit richtigen und falschen Antworten aufgenommen wurde. Unsere Ergebnisse zeigten, dass die Hauptveränderliche bei der Feststellung aufgabenbezogener Änderungen in der Spike-Field-Kohärenz die Verhaltensleistung war.

Geschätzt wurde die Spike-Field-Kohärenz mit der Multitaper-Methode, welche eine optimale Konzentration spektraler "Power" erlaubt und dadurch den Leakage-Effekt minimiert. Um der niedrigen Anzahl Spikes zu begegnen, welche im präfrontalen Kortex bei weniger als 1 – 5 Spikes pro Sekunde liegen kann, entwickelten wir einen kombinierten Ansatz, mit welchem wir die Zuverlässigkeit der Veränderungen in der Spike-Field-Kohärenz in experimentellen Daten schätzen sowie die Dynamik des zugrundeliegenden Prozesses quantifizieren können. Unser Ansatz setzt sich aus drei Schritten zusammen. Der erste Schritt besteht in der Multitaper-basierten Analyse leistungsbezogener Veränderungen in der Spike-Field-Kohärenz in experimentellen Daten. Im zweiten Schritt formulierten wir ein Modell für die zeitliche Koordinierung von Spike- und LFP-Signalen, simulierten künstliche Daten anhand des Modells und wendeten schließlich die selbe Analyse auf die simulierten künstliche

Daten an, um die Zuverlässigkeit der experimentellen Ergebnisse zu untersuchen.

Die Multitaper-Methode ist eine spezielle Spektral-Analyse, die angewendet wird, um die Leakage zu reduzieren und die Power zu konzentrieren. Der direkte spektrale Schätzer ist stark verzerrt, wenn der Prozess über eine große dynamische Spannbreite verfügt. Die Multitaper-Methode überwindet dieses Problem, indem sie die spektralen Schätzer von verschiedenen orthogonalen Tapers mittelt. Darüber hinaus können die Verzerrung und das Konfidenz-Intervall der Analyse nach der Anwendung der Multitaper-Methode auf einfache Weise geschätzt werden. Wir wendeten die Multitaper-Methode auf Daten zum Kurzzeitgedächtnis von Affen an, und es zeigte sich, dass bei hinreichend großem Datenumfang das zusätzliche Glätten der Multitaper-Methode nicht nötig ist, um die Varianz zu verringern oder wichtige Frequenz-Komponenten sichtbar zu machen.

In einem letzten Schritt schätzten wir die statistische Signifikanz der verhaltensabhängigen Unterschiede in der Spike-Feld-Kohärenz. Dazu nutzten wir Permutationstests. Permutationstests sind nicht-parametrische statistische Instrumente. Sie liefern eine einfache und zuverlässige Methode, die  $H_0$ -Hypothese ohne zusätzliche mathematische Annahmen abzuleiten. Diesen Signifikanztest wendeten wir auf jedes Paar von Spike und lokalem Feld-Potential an und berechneten anschließend wie viele der gesamten Paare von Spikes und lokalen Feld-Potentialen je Experiment eine signifikante Erhöhung oder Verringerung bei richtigen oder falschen Antworten zeigten. Diesen Wert bezeichnen wir als  $\lambda$ -Wert für die verschiedenen Antworten des Affen. Als ersten Befund stellten wir fest, dass die Veränderung des  $\lambda$ -Werts für unterschiedliche Frequenzen sehr unterschiedlich ausfällt. Als zweites fanden wir, dass der  $\lambda$ -Wert für Spike-Field-Kohärenz-Unterschiede im Hochfrequenz-Band (25 – 70 Hz) für experimentelle und für simulierte Daten vergleichbar

war: 3,5% bzw. 2,7%. Das gleiche gilt für den mittleren Basiswert von  $\lambda$  und seine Variabilität in den experimentellen und simulierten Daten. Daher zeigte die Analyse beider Datensätze die gleiche, als Änderung der z-Punktzahl von etwa 40 ausgedrückte, maximale relative Modulation von  $\lambda$ . Dies macht deutlich, dass, obwohl die Variabilität der individuellen Schätzer für Spike-Field-Kohärenz recht hoch sein kann, die auf einer hohen Zahl von Schätzern basierende Bewertung leistungsbezogener Unterschiede in  $\lambda$  sehr zuverlässig ist. Quantitative Vergleiche der beiden Typen simulierter Daten, wobei der eine Phasengenauigkeit und der andere Synchronisationsstärke modelliert, zeigten, dass experimentelle Ergebnisse im Hochfrequenz-Band höchstwahrscheinlich auf präzisen, phasengekoppelten Spikes basieren, welche mit kleiner Häufigkeit auftreten. Angesichts der Analyseergebnisse bei den simulierten Daten müssen Spikes mit einer Präzision von weniger als 2 ms an LFP-Oszillationen von 50 Hz (Phasen-Genauigkeit  $0,2\pi$ ) gekoppelt sein, um  $\lambda$ -Werte nahe der in den experimentellen Ergebnissen beobachteten maximalen Werte (3,5%) zu erreichen. Angesichts der eher kurzen Periode ( $w = 2$  ms), einer Oszillationsfrequenz von 50 Hz und einer Rate  $r_1 = 25$  Spikes/Sekunde erwarten wir 0,5 phasengekoppelte Spikes pro Analysefenster. Dies illustriert erstens die hohe Sensitivität der Methode und zweitens, dass, obwohl Unterschiede zwischen Verhaltenszuständen auf eher wenigen Ereignissen phasengekoppelter Spikes zu beruhen scheinen, die aufgabenbezogenen Effekte auf die Spike-Field-Kohärenz hoch-zuverlässig sind und nicht durch Zufall erklärt werden können, wie der Vergleich der Analysen von experimentellen und von simulierten Daten zeigt. Die differentielle Kopplung von präfrontalen Neuronen-Populationen mit zwei verschiedenen Frequenzbändern in ihren Eingangssignalen legt es nahe, dass die dem Kurzzeitgedächtnis im präfrontalen Kortex zugrunde liegende neuronale Aktivität vorübergehend kortikale Kreisläufe auf verschiedenen räumlichen Skalen nutzt, und dies ver-

mutlich mit dem Zweck, verteilte Prozesse zu koordinieren. Des weiteren erklärt die präzise Kopplung zwischen Spike- und LFP-Oszillationen während Verhaltensübergängen, dass vorübergehende Koordination zwischen lokalen, mikroskopischen und globaleren, entweder mesoskopischen oder makroskopischen Kreisläufen während Gedächtniskodierung und -abfrage nötig sein könnte. Zweitens untersuchten wir verschiedene Muster in Spike-Feuerraten, welche auf die Verhaltensleistung des Affens zurückzuführen sind. Neuronale Aktivitäten im Kurzzeitgedächtnis wurden mit anhaltenden Erhöhungen der Feuerraten von Neuronen im präfrontalen Kortex assoziiert. Es ist jedoch unklar, auf welche Weise große Populationen von Neuronen Informationen aufeinander abgestimmt abspeichern.

Um die Bedeutung von synchronem Feuern in Bezug auf Informationsverarbeitung im Gehirn zu testen, ist zu untersuchen, ob synchrones Feuern und seine Stärke mit dem Zustand des neuronalen Systems oder dem Verhalten und der Aufgabe des Probanden korrelieren. Dies erfordert ein Instrument, welches die Stärke des synchronen Feuerns über mehrere Zustände (‚Faktoren‘) hinweg vergleichen kann, während es gleichzeitig andere Merkmale neuronalen Feuerns wie Spike-Raten-Modulationen oder die Autostruktur der Spike-Aktivität, die gemeinsam mit synchronem Feuern auftreten könnten, berücksichtigt. Die bisherige Methode NeuroXidence ist für den univariaten Fall konzipiert und wurde optimiert, um synchrones Feuern, welches über das erwartete Maß hinausgeht, zuverlässig zu erkennen. Sie erlaubt es jedoch nicht, die Stärke über Faktoren hinweg zu vergleichen.

Wir stellen hier eine bi- und multivariate Erweiterung von NeuroXidence vor. Diese Erweiterung erlaubt es, für ein festes Spike-Muster den Umfang synchronen Feuerns in verschiedenen Faktoren zu vergleichen. Diese Erweiterung ist robust gegenüber Ratenveränderungen einzelner Neurone und gegenüber Raten-Kovariation von Neuronengruppen. Sie berücksichtigt die gesamte Au-

tostruktur ebenso wie Variabilität über einzelne Durchgänge.

Die grundlegende Idee der bi- und multivariaten Erweiterung ist die, zunächst die Häufigkeit gewisser Aktivitätsmuster gleichzeitig aktiver Neurone (”Joint-Spike-Events” (JSEs)) für jeden Durchgang und für jeden Faktor des Experiments zu bestimmen. Dann werden Ersatz-Daten (’,Surrogate’) erzeugt, bei denen jeder Ersatz-Spiketrain identisch ist mit dem entsprechenden ursprünglichen Spiketrain, bei denen aber jegliche feine zeitliche Quer-Struktur zwischen simultan aufgenommenen Spiketrains durch Verschieben (’,Jittern’) des gesamten Spiketrains um eine zufällige Zeit zerstört wird. Hierzu definieren wir zwei Zeitskalen. Die erste,  $\tau_c$ , definiert die erwartete Präzision von JSEs und beträgt in der Regel wenige Millisekunden. Die zweite Zeitskala,  $\tau_r$ , ist um ein  $\eta$ -faches langsamer als  $\tau_c$  und definiert die untere Schranke der Raten-Modulation.

Diese Ersatz-Daten dienen uns als Schätzung für die Häufigkeit zufälliger JSEs unter der  $H_0$ -Hypothese, dass Neuronen nicht auf einer feinen zeitlichen Skala gekoppelt sind. So nutzen wir also die Häufigkeit der JSEs in den Ersatzdaten, um die Häufigkeit der JSEs in den ursprünglichen Daten zu korrigieren. Wir berechnen die Differenz zwischen der Häufigkeit im ursprünglichen und im Ersatz-Datensatz für jeden Versuchsdurchgang und jeden Faktor. Unterschiede, welche auf unterschiedliche Faktoren zurückzuführen sind, werden durch bivariate Mittelwert- oder Mediantests (t-Test und Mann-Whitney U-Test) oder durch Varianzanalyse-Tests im multivariaten Fall aufgedeckt. Der p-Wert gibt an, wie gut Modulationen des synchronen Feuerns auf der Zeitskala  $\tau_c$  über Faktoren hinweg durch Zufall erklärt werden können.

Bevor wir die Methode auf die experimentellen Daten anwenden, kalibrierten wir die Erweiterung von NeuroXidence für bi- und multivariate Fälle. Dazu verwendeten wir die simulierten Daten. Besonders bei nicht-stationären Prozessen sortiert NeuroXidence Artefakte aus, die verschiedene Prozesse ( $\gamma$ -



Prozess, Poisson-Prozess und Latenzzeit-Kovariationen von Aktivitätsmodulationen) in Bezug auf die Häufigkeiten von JSEs produzieren können.

Was die Test-Power betrifft, so können im Mittel Unterschiede von nur 3 JSEs in verschiedenen Zuständen entdeckt werden, was von der hohen Sensitivität von NeuroXidence in bi- und multivariaten Fällen zeugt. Wenn es darum geht, JSEs in Prozessen mit verschiedenen Rateniveaus aufzuspüren, spielt neben den Parametern  $\tau_c$  and  $\tau_r$  die Anzahl  $S$  der Ersatz-Daten eine wichtige Rolle. Wenn NeuroXidence auf zwei Prozesse oder mehr angewendet wird, die unterschiedliche Raten aufweisen, und insbesondere wenn einige der Prozesse eine niedrige Feuerrate besitzen, sollte die Anzahl  $S$  an Ersatz-Daten auf 1 gesetzt werden, um unverzerrte Schätzer für die JSEs zu erhalten.

Kurz zusammengefasst konnten wir zeigen, dass die Anwendung von NeuroXidence auf die Kurzzeitgedächtnis-Daten aufgenommen im Affen einen signifikanten Anstieg von JSE-Mustern, die von der Aktivität von bis zu 7 Neuronen gebildet werden und vermehrt in den Versuchsdurchgängen auftreten, in denen der Affe richtig antwortete, ergab. Besonders spannend war der zeitliche Verlauf dieser Erhöhungen. Es zeigten sich Erhöhungen vor allem während Zeitintervallen, in denen Informationsverarbeitung, Informationsverschlüsselung und Informationserhaltung notwendig sind.

In einem letzten Schritt verglichen wir die Ergebnisse der verhaltensabhängigen Modulation der Spike-Feld-Kohärenz und der Spike-Spike-Synchronisation, um Interaktionen auf verschiedenen räumlichen Skalen vergleichen zu können. Beide Analysen zeigen konsistente Erhöhungen oder Verringerungen, so dass wir auf eine enge Beziehung zwischen den Aktivitäten auf verschiedenen räumlichen Skalen schließen können.

# Content

<b>1</b>	<b>Introduction</b>	<b>3</b>
1.1	Neural signals: spike and local field potentials . . . . .	3
1.1.1	Spike . . . . .	3
	Generation of spikes . . . . .	4
	Electrode recording . . . . .	5
	Spike sorting . . . . .	5
	Spike and point process . . . . .	6
1.1.2	Local field potential . . . . .	6
1.1.3	Relations between slow wave signal and spike activity . . . . .	7
1.2	Tools to analyze spike signal . . . . .	8
1.2.1	Cross-correlogram . . . . .	8
1.2.2	Spectral analysis . . . . .	9
1.2.3	Spike pattern classification methods . . . . .	10
1.2.4	Likelihood method . . . . .	10
1.2.5	Information theory . . . . .	11
1.3	Prefrontal cortex and its function . . . . .	12
1.3.1	Study on human prefrontal cortex . . . . .	12
1.3.2	Study on monkey prefrontal cortex . . . . .	13
<b>2</b>	<b>Spike-field coherence in monkey prefrontal cortex</b>	<b>17</b>
2.1	Introduction . . . . .	17
2.2	Experiment on monkey prefrontal cortex . . . . .	18

<i>CONTENT</i>	ix
2.3 Methods for analyzing spike-field coherence . . . . .	20
2.3.1 Spectral analysis: Multitaper method . . . . .	20
2.3.2 Significance test: Permutation test . . . . .	23
2.3.3 $\lambda$ -maps . . . . .	24
2.4 Results of experimental data . . . . .	25
2.5 Simulated-data model and method calibration . . . . .	29
2.6 Discussion . . . . .	34
2.7 Summary . . . . .	34
<b>3 Bi- and multi-variate spike train analysis</b>	<b>36</b>
3.1 Introduction . . . . .	36
3.2 Method . . . . .	37
3.3 Method calibration (Part I) . . . . .	39
3.3.1 False positives for two stationary processes . . . . .	39
3.3.2 Test-power for stationary process . . . . .	42
3.3.3 Sub- and Supra-patterns of induced JS-patterns . . . . .	44
3.3.4 False Positives for a non-stationary process . . . . .	44
3.4 Method calibration (Part II) . . . . .	47
3.4.1 False positives for stationary processes . . . . .	47
3.4.2 Test power for multivariate case . . . . .	48
3.5 Results of JSEs in short-term-memory experiment . . . . .	52
3.6 Spike-spike coherence and joint-spike-event . . . . .	60
3.7 Discussion . . . . .	62
3.8 Summary . . . . .	64
<b>4 Discussion</b>	<b>65</b>
4.1 Multitaper method, permutation test and NeuroXidence . . . . .	65
4.1.1 Multitaper method . . . . .	65
4.1.2 Permutation test . . . . .	66

<i>CONTENT</i>	x
4.1.3 NeuroXidence method . . . . .	66
4.2 Short-term memory process in monkey prefrontal cortex . . .	67
<b>5 Conclusion</b>	<b>70</b>
5.1 Scale Integration . . . . .	70
5.2 NeuroXidence method and Synchronized firing . . . . .	71
<b>A Appendix: Coherence</b>	<b>72</b>
<b>B Appendix: Bonferroni correction</b>	<b>74</b>
<b>Acknowledgement</b>	<b>89</b>
<b>Curriculum Vitae</b>	<b>90</b>

# Abstract

To investigate neuronal processing during short-term memory, we recorded simultaneously local field potentials and spikes from prefrontal cortex of two monkeys, who performed a visual short-term memory task. Then, we applied two different methods to analyze these two signals.

First, we analyzed the behavior-related modulations of coupling between signals on two spatial scales: very local multi-unit activity and local field potentials. Coupling was assessed by spike-field coherence based on multitaper method. To overcome limitations of spike-field coherence estimates in case of low firing rates, we developed a new method that estimates the percentage of pairs of spike and local field potential signals that expressed differences between behavioral conditions, here trials with correct or incorrect responses. Based on simulated data, we demonstrated that the new method allows for a reliable estimation of differences in spike-field coherence, even in case of very low firing rates. Application to recordings in prefrontal cortex of two monkeys revealed that locking of spikes was differentially modulated with two different frequency bands depending on behavioral performance.

Second, we studied the difference of spike firing patterns due to monkey's behavioral performance. We extended the NeuroXidence method (Pipa et al., in press.) to detect joint-spike events in bi- and multi-variate cases. Based on simulated data, we verified the reliability and sensitivity of NeuroXidence for detecting joint-spike events among several conditions. After application

to the short-term-memory data set, the results showed the difference in firing patterns during the early delay of the task. Comparing the results with that of spike-spike coherence, we demonstrate that NeuroXidence method is a good way to detect more than pair-wise relations of spike trains.

**Key words:** *short-term memory, oscillations, scale integration, spike-field coherence, multitaper estimation, bootstrapping permutation test, monkey pre-frontal cortex, joint-spike event, NeuroXidence method, spike-spike coherence*

# Chapter 1

## Introduction

### 1.1 Neural signals: spike and local field potentials

There are more than 100 billion neurons in the human brain. Neurons are interconnected by synapses, which transfer information among neurons and from one part of the brain to another. Neurons also form a network to enable people to feel the world and control their behavior. To understand and explain people's behavior, one needs to study the activities of the brain. Therefore many different signals in the brain are recorded and analyzed. Spikes and local field potentials are two of the most interesting signals.

#### 1.1.1 Spike

In order to transfer information from one neuron to another, electrical pulses are generated by a neuron and are transferred rapidly along long nerve fibers. This electrical pulse is called an action potential or spike ([1], [2]).

## Generation of spikes

Each neuron has four characteristic parts: the cell body (soma), the dendrites, the axon, and presynaptic terminals. Neurons receive inputs on dendrites and transfer spikes along axons to presynaptic terminals. Because of the branching structure of the dendritic tree, neurons can receive inputs from many other neurons. There are many different ion channels on dendrites, which allow the ions (sodium ( $Na^+$ ), potassium ( $K^+$ ), calcium ( $Ca^{2+}$ ), chloride ( $Cl^-$ )) to flow in and out of the cell. The direction of the ion flow is determined by voltage and concentration gradients. Under resting conditions, the inside potential of the neuron is about  $-70$  mV lower than that of the outside. If the flow of the ions into the neuron is sufficient to raise the membrane potential above a threshold level, an action potential is generated by the neuron (Fig. 1.1).

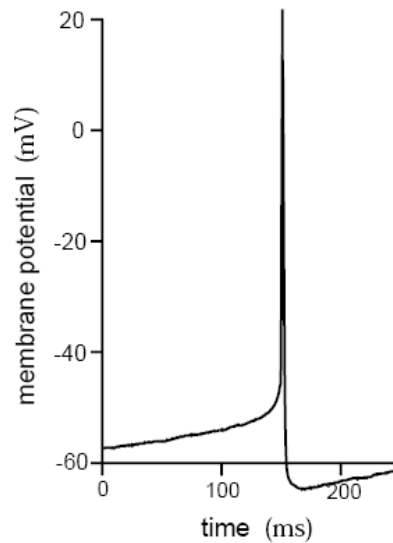


**Figure 1.1:** An action potential recorded intracellularly from a cultured rat neocortical pyramidal cell ([3]).



## Electrode recording

There are generally two ways of recording spike signals: intracellular recording and extracellular recording. In Fig. 1.2, an electrode is placed quite near a neuron but it does not pierce the membrane. Such recordings can detect the action potentials fired by the neuron, but not its subthreshold membrane potentials. Extracellular recordings are typically used in vivo experiments. Intracellular recordings are sometimes used in vivo, but are more often used in vitro preparations and experiments.

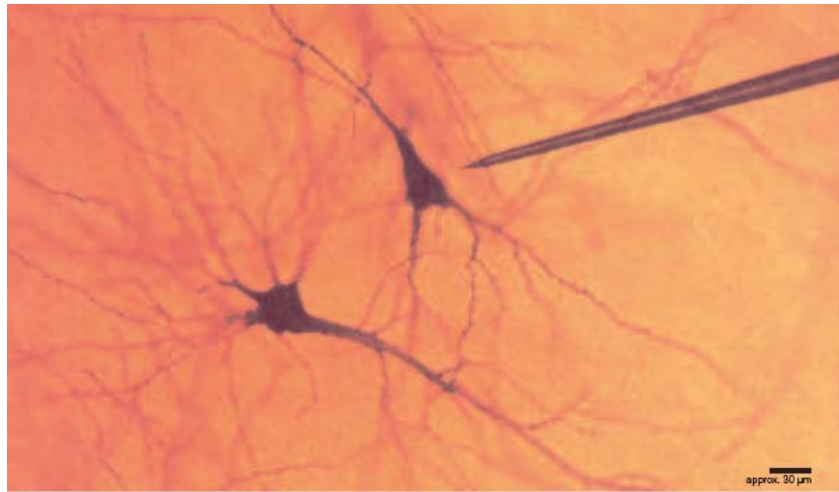


**Figure 1.2: Extracellular recording in the tissue.**

## Spike sorting

As shown above, in the extracellular recording, individual spikes are not directly recorded. When multi-electrodes or tetrodes are implanted, each electrode will record the electrical activities from an unknown number of neurons. From these recorded electrical activities, the number of neurons must be determined. Each spike must be separated from others, and each spike must be assigned to the neuron that generates it ([4, 5, 6]). This process is called 'spike sorting'. The accuracy of the spike sorting could affect a lot on the accuracy

of all subsequent analyses.

Many algorithms have been developed for spike sorting, and until now, none of them is better than the others. Different algorithms applied to the same dataset can get different results, which shows the complication of the spike sorting. Meanwhile, it is quite hard to identify the number of neurons. One could assume a number of neurons, usually larger than the believed number, and later combine the clusters that are close enough ([6]). Also, for different numbers of multiple electrodes or multiple electrodes with different geometries, it is hard to find a general spike-sorting algorithm.

### **Spike and point process**

Since spikes have a characteristic shape, people believe that only the sequence of time points, when the neuron generates its action potentials, contains the information which is transferred by a neuron. Thus, people usually neglect the detailed structure of the spike unless one is interested in the intracellular spike-generating mechanism or distinguishing the activities of one neuron from others. Hence, the most common way to study spike trains is that spikes are treated as sequences of time points, which show the occurrence of the spikes. In mathematics, such process is called a 'point process'.

#### **1.1.2 Local field potential**

In extracellular recordings, the spikes are not recorded directly. Because of the geometry and the symmetry of the alignment of neurons, the electrodes record the activities of a number of neurons. Such unfiltered signal reflects not only the sum of action potentials from different neurons ([7]; [8]), but also the slow ion flow current ([9]). Then the signal is low-pass filtered, cut off at  $\sim 300$  Hz, to obtain the local field potential.

Since the local field potential is a low-pass-filtered signal, fast changes in

the potential are filtered out, and only the slow changes remain. The fast changes are caused by the currents of the action potential. Thus the local field potential contains no information of the spike signal, and it only reflects the local sustained ionic current in the tissue. The major slow current is the postsynaptic potential. Due to these properties of local field potential, it is believed that the local field potential reflects the input into the observed area, which is different from the spike signal, which represents the output from the area.

### **1.1.3 Relations between slow wave signal and spike activity**

As described above, spikes reflect the output of the neurons that transfers information among the neurons, while local field potentials contain information of neuronal synaptic activities. The relations between these two signals become interesting for two reasons. First, it is important to relate the spike activity with continuous processes, which represent either stimuli or the responses to them. When the continuous signal represents the stimuli, the relation between neural responses and stimuli could tell more about the neural unique responses to different stimuli and help people to understand the function of spike activity. On the other hand, the continuous signal could also represent responses to spike activity, such as the movements of joints that are driven by the spikes generated by motoneurons. Such study of relations between stimuli and response of the two types of processes could help people to know more about the neural system function and help to build more reasonable mathematical models of nervous system. The second reason for studying the relations between these two types of processes is that they provide a way to study the slow-wave and spike activity that can always be detected in the brain, especially when there are no external stimuli. The relations between

these two types of electrical signals are one of the most fundamental studies to understand nervous system functions. To figure out these relations, analyses that are suited to both continuous and point processes should be applied. Among these analyses, spike-field coherence is a good choice. Although it is a linear relationship between these two signals, it still can provide the preliminary description of relations that are thought to be nonlinear([10]).

## 1.2 Tools to analyze spike signal

With the development of experiment techniques, people now can control a stimulus and record simultaneously neural activities from part of the brain, which is thought to be the response to the stimulus. The stimulus could be physical in nature, such as light used to stimulate retinal, or sound used to stimulate neural activity in the auditory cortex. Also, the stimulus could be abstract, such as in a short-term memory task, where the stimulus causes neural activities in prefrontal cortex. With the development of multi-electrode recording ([11]), people now can study the simultaneous spiking activity of many neurons. Thus, it helps to understand how groups of neurons could coordinate with each other and transfer information from one part of the brain to other regions. Such studies bring up the problem of how to analyze the multiple simultaneously recorded spike trains in a proper way.

### 1.2.1 Cross-correlogram

Most current methods for neural spike-train analysis concern only relations between pairs of neurons. These methods can be divided into two types: time-domain and frequency-domain analysis. Among time-domain analysis, the most commonly used method for measuring relations between neurons is the cross-correlogram. The cross-correlogram is a function that computes the

cross-covariance between two spike trains with a pre-assigned bin width. To apply this method, it requires that the two spike trains are stationary. In other words, it is required that the stochastic properties of the neurons do not change in time. In many cases, the 'stationarity' property of the spike trains can not be guaranteed, since the neural responses are caused by time-varying stimuli, and the responses to the same stimulus could also change in time. However, non-stationarity can be solved by performing the analysis in moving windows.

### 1.2.2 Spectral analysis

If we assume the stationarity property of the neurons, frequency-domain analysis of the neural signals can be achieved by taking the Fourier transform of the signals. Based on the spectra of the signals, cross-spectra or coherence between signal pairs could be accessed ([10], [12], [13],[14]). The coherence is a simple frequency-dependent relation between two processes, which is computed by the auto- and cross-spectra of the signals. Compared with time-domain analysis, coherence has two advantages: the normalization does not depend on bin size, and it can reveal linear pair-wise relations among all the neuron pairs. At the same time, coherence can be applied both to point processes and continuous-valued processes. Thus it allows for the study of the linear relations in each process and those between two processes. Since the non-stationarity is an important feature of spike signals, the time-frequency spectra can be assessed by moving-window estimates ([15]). Some time-domain functions could also be computed by inverse Fourier-transforming the corresponding frequency-domain functions.

### 1.2.3 Spike pattern classification methods

Since the methods mentioned above only concern the pair-wise relations between neurons, there are also many algorithms that can detect different patterns of multiple neuronal spike trains ([16], [17], [18]). These methods can evaluate the high-order neural relations ([19]) and tell more about the synchronized firing of the neurons. For instance, some method could achieve the statistical significance of spike triplet occurrences or that of similar patterns among many neurons ([20]). Meanwhile, methods for detecting statistically distinct spike patterns have also been developed. Such patterns are called 'unitary events' or 'joint-spike event', when the occurrences of the patterns are statistically significant more than that expected by chance ([21], [22], [23]). The occurrence of different spike patterns is studied in relation to behavioral events or different stimuli. These spike-pattern classification methods require that the complexity or size of the patterns should be chosen, the null hypothesis should be assessed in a proper way, and the test statistic should be formulated. Thus it can evaluate the correct significance level of the spike patterns afterwards.

### 1.2.4 Likelihood method

Likelihood methods are the most important tools for modeling and analysis in statistical research ([24]). They can also be applied in neuroscience data analysis. Most likelihood methods require a specific parametric probability model for the studied process. Under the assumption of the model, the likelihood is defined as the joint probability density of the data from the process, which is a function of the model's unknown parameters. The unknown parameters can be estimated later from the experimental data by formal procedures such as the maximum likelihood method. If the probability model assumed before is a good approximation to the process, the likelihood method then can

provide an optimal way to analyze the experimental data ([24]). Meanwhile, likelihood methods can also be applied to spike-train analysis, both for single spike-train analysis ([12], [25], [26], [27], [28]) and for multiple spike-train analysis ([12], [29]). Since multiple neural spike trains imply multivariate point processes in the analysis, the challenge in applying likelihood methods to multiple spike-trains analysis is to build a proper model that represents the joint-spiking activity and to develop an algorithm to judge the model's goodness-of-fit ([29]).

### 1.2.5 Information theory

Information theory measures are widely used in analysis of neural spike trains ([30], [31], [32], [33]), such as entropy to measure spike train variability, and mutual information to study the relations between two spike trains. Information theory measures use single numbers to describe the complicated relations between spike trains. These measures, which usually estimate the relevant probability densities, have been applied to study how much information a single spike train can transfer. The basis of these methods is that some parts of the nervous system, such as visual pathways, could be modeled as communication channels ([30]) with some underlying principles. When these methods are applied, usually the details of the system properties are left out. However, there are limitations to this approach. For any neural system, the optimal 'word' length is unknown and must be estimated. Thus different word lengths could bring different results, and longer word requires large amount of experimental data ([33]). Moreover, whether the nervous system can be treated as conventional communication channels has been questioned ([35]).

## 1.3 Prefrontal cortex and its function

The cerebral cortex plays a central role in many complex brain functions, including language, cognition, and memory. In each cerebral hemisphere, from an anatomical view, the cortex is divided into four distinct lobes: *frontal*, *parietal*, *temporal*, and *occipital* (Fig. 1.3). The prefrontal cortex lies in the anterior part of the frontal lobes of the brain.

These four lobes have different functions. The frontal lobe is involved with planning and partly motor function; the parietal lobe with integrating sensory information from various parts of the body; the occipital lobe with vision; and the temporal lobe with hearing.

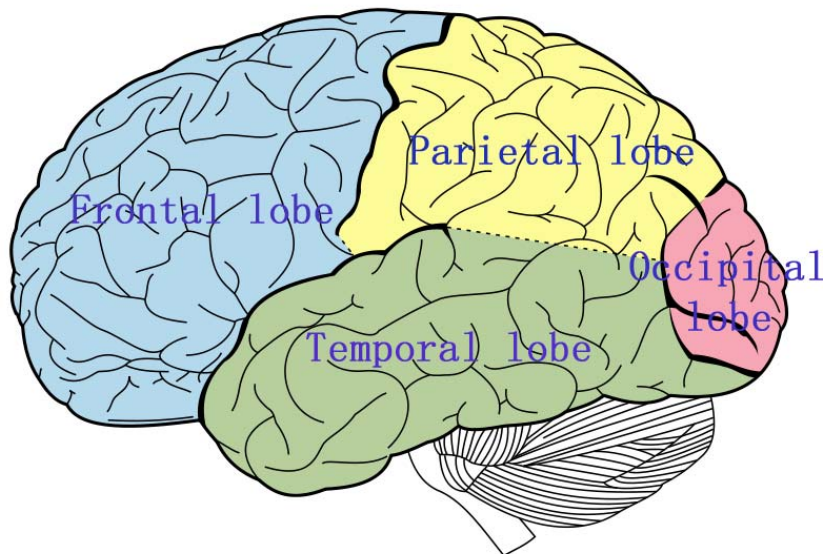


**Figure 1.3:** The four lobes of the cerebral cortex.

### 1.3.1 Study on human prefrontal cortex

The classic study of human prefrontal cortex function in the nineteenth century involved an accident of Phineas Gage. A tamping iron was driven through Gage's frontal lobes by an explosion. After the accident, he survived and had



no problems with talking, walking or normal memory. However, due to injury to his prefrontal cortex, his personality was remarkably changed. From then on, he could not manage his work or personal life in a proper way.

Subsequent studies have shown that the patients who have prefrontal injuries can describe the proper behavior under certain circumstances, but when actually performing, they only care for the instant satisfaction and have no consideration of the long-term results.

These results indicate that the prefrontal cortex has the function of comparing the instant satisfaction with the more rewarding long-term satisfaction and the function of making the correct choice. It shows that the prefrontal cortex plays a central role in long-term planning and judgement.

### **1.3.2 Study on monkey prefrontal cortex**

In the nineteenth century, some researchers made experiments on the monkeys without the prefrontal cortex ([37]). Based on the observations of these experiments, the experimental psychologists made the conclusion that the prefrontal cortex is involved in intellectual and cognitive, rather than sensory or motor, functions. Later, more structured and comparative studies were carried out to investigate the effect of frontal lesions. Some researchers argued that with the removal of the frontal lobes, it becomes difficult for the animal to gather various incoming percepts and make further motor commands ([38]). Other researchers applied objective behavioral testing methods to study the effects of the frontal lobe removal ([39]). However, they all failed to build a proper framework of what role the prefrontal cortex might play in high-level cognition. They couldn't find a reliable and proper way to investigate and capture the relations between an animal's behavior and the prefrontal lesions. The delayed-response task (Fig. 1.4) that Jacobsen ([40]) and Hunter ([41]) used in experiments became the cornerstone of study on prefrontal lesion.

Jacobsen's theory described the delayed-response and visual discrimination capabilities of monkeys that had been tested in prefrontal, pre-motor, or temporal lobe lesions. He found that only monkeys with prefrontal lesions showed a selective and delay-dependent deficit on delayed-response tasks. Delayed-response tasks examine the animal's ability to maintain the information of the stimulus over a period of delay. When the animal is asked to make a choice, the related information must guide the behavior to give the correct response, since there were no other signals for that. Based on these ideas, Jacobsen made the conclusion that the deficit due to prefrontal lesion was related to memory process. Specifically, the monkey's ability to use 'immediate memory' to guide its behavior was damaged by the prefrontal removal.

Based on the work of Goldman-Rakic ([42], [43], [44], [45], [46], [47], [48], [49]), damage to the dorsolateral prefrontal cortex (Fig. 1.5), causes great deficits in spatial working memory. Performance is generally unchanged on tests of non-spatial short-term memory, unless executive control processes are required, as shown by Petrides ([50]).

Some evidence shows that lesions to the ventrolateral prefrontal cortex may result in non-spatial short-term memory deficits. However, there are several problems with this explanation: First, no study has shown a selective deficit in the spatial as compared with the non-spatial domain. When deficits were found in the spatial domain, they also occurred in the non-spatial domain. Second, there is no study on the relation between deficits and the delay period. Third, damage to the ventrolateral prefrontal cortex also causes deficits with the tasks that require no short-term memory process([53], [54], [55], [56]). Therefore, deficits caused by ventrolateral prefrontal cortex lesions may be better explained as an incapability to form and/or use associations between cues and motor responses, or may be more associated with incapability to use learning strategies ([57]).

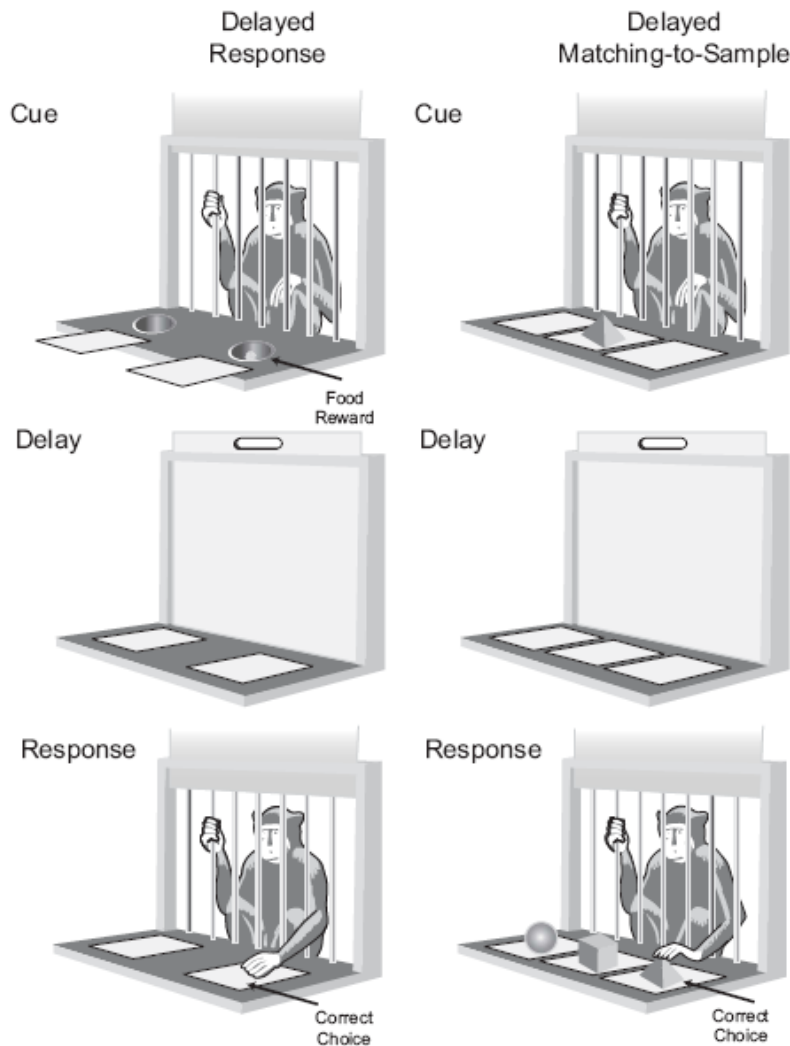


**Figure 1.4: Schematic description of short-term memory tasks used to test the function of prefrontal cortex.** The spatial delayed-response task (left) is focused on spatial short-term memory and requires the monkey to remember the baited location of a food well over a delay. The delayed matching-to-sample task (right) is a non-spatial working memory task and requires the monkey to remember an object over a delay. After the delay, only the well beneath the sample object is baited. A common variant (not shown) is the delayed non-matching-to-sample task, in which the monkey remembers the sample object, but after the delay must select an object that does not match the sample object's form.

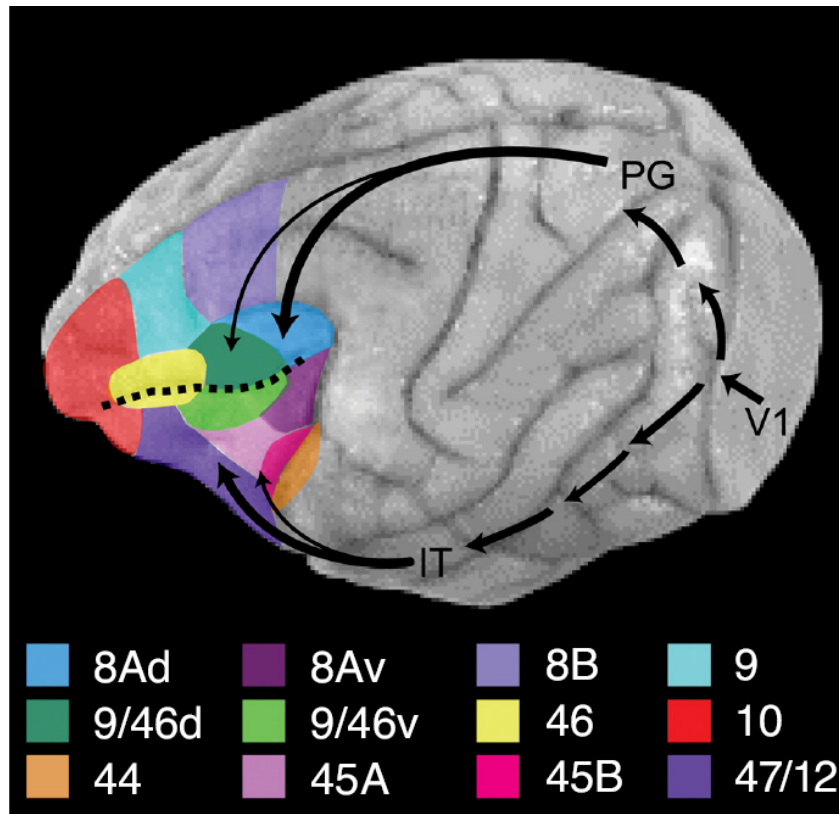


**Figure 1.5: Subdivisions of the macaque prefrontal cortex as defined by Petrides and Pandya ([51]).** The mid-dorsolateral prefrontal cortex is composed of areas 46 and 9/46d, and mid-ventrolateral prefrontal cortex of areas 47/12, 45A, and 9/46v. Also shown are the dorsal and ventral streams that respectively process spatial and non-spatial visual information ([52]).

# Chapter 2

## Spike-field coherence in monkey prefrontal cortex

### 2.1 Introduction

Mechanisms of information processing involve neuronal circuits at various spatial scales ([58], [59], [60], [61], [62], [63], [64], [65], [66], [67], [68]). Their contributions can be studied by analyzing different signals like single units, populations of neurons, local field potential and other mass signals. Interactions between these different levels are particularly interesting if information processing is subject to behavioral transitions or state changes, even if they are subtle. In this chapter we tested whether the relation between synaptic inputs - as reflected in the local field potentials - and the spiking output of local neuronal populations in lateral prefrontal cortex changes, when perceived information needs to be stored and recalled later when comparison to new sensory input, is the basis for choosing the appropriate behavioral response. As spike-field coherence has been shown to change dynamically with memory processing [69, 70, 71], we analyzed spike-field coherence computed from simultaneously recorded local field potential and multi-unit activities in lat-

eral prefrontal cortex of two monkeys performing a visual short-term memory task (0.5 second sample, 3 seconds delay, 2 seconds test presentation; Fig. 2.1). The primary variable for assessing task-related changes of spike-field coherence was behavioral performance, for which we compared trials with erroneous responses to a matched set of trials with correct responses. Spike-field coherence was assessed with a multitaper method [14, 72] that allows for an optimal concentration of spectral power and therefore minimizes the effect of leakage. To overcome the low number of spikes, which can be as low as 1 – 5 spikes per second in the prefrontal cortex, we developed a combined approach with which we can estimate the reliability of spike-field coherence modulations in experimental data as well as quantify the dynamics of the underlying neuronal process. Our approach consists of three steps. The first step is the multitaper-based analysis of performance-related spike-field coherence modulations in experimental data. In the second step, we formulated a model for the temporal coordination between the spike and local field potential signals, and applied the same analysis as on the experimental data to investigate the reliability of the experimental results. In a third step, we modified the temporal correlation in the model and compared these results with the results of the experimental data.

## **2.2 Experiment on monkey prefrontal cortex**

Two adult female rhesus monkeys (*Macaca mulatta*), weighing 6 and 8 kg, were implanted with head bolts and recording chambers over lateral prefrontal cortex around the posterior half of the principal sulcus, mostly ventral of the principal sulcus. Stimulus presentation and behavioral control was provided by a custom-made program running under DOS. Anatomical MRI scans (T1-flash) were performed on a 1.5T magnet and used to guide implantation of recording chambers and reconstruct recording positions (Fig. 2.2). Eye move-

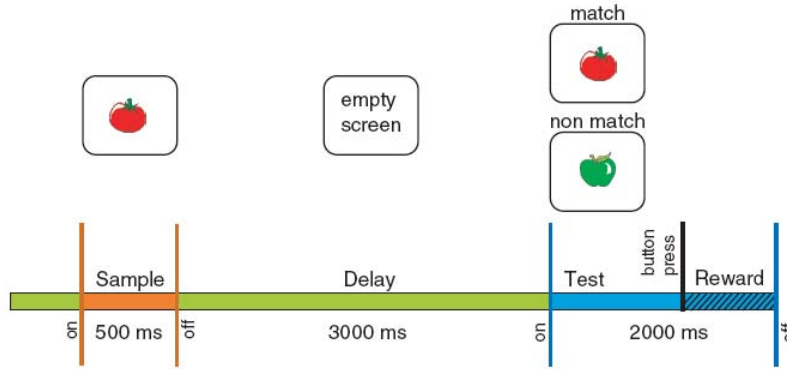


**Figure 2.1: Time course of visual short-term memory task** ([76]). After a 0.5 – 1 second baseline, a sample stimulus was presented for 500 ms which was followed by a 3 seconds delay. Then a test stimulus was presented for 2 seconds during which the monkey had to respond by a differential button press. In case of a matching test stimulus, the monkey had to press the left of two buttons, and the right button should be pressed if a non-matching test stimulus is shown. This visual memory task combines the classical matching-to-sample and non-matching-to-sample tasks. The reward was delivered after the monkey released the button which happened on average 200 – 300 ms later.

ments and all behavioral responses were recorded at the same resolution as neuronal signal[73]. All procedures were performed in accordance with the German Law for the Protection of Experimental Animals and NIH guidelines. We used up to 16 individually movable platinum-tungsten fiber microelectrodes (Thomas RECORDING GmbH, Giessen, Germany) that were arranged in an array with 500  $\mu\text{m}$  spacing. The spacing of the matrix was chosen to approach the spacing of microcolumns in lateral prefrontal cortex [74]. Signals, digitized at 1 kHz, were preprocessed by rejecting artifacts (movements, licking) and removing line noise at  $50 \pm 0.5$  Hz. Local field potentials and

multi-unit activities were recorded from the same microelectrodes by employing two band-pass filters (5 – 150 Hz, 0.5 – 5 kHz, 3 dB/octave). In total, we could analyze 4124 trials in 12 sessions (1593 pairs) for two monkeys. On average, the monkeys gave correct responses in 80% of the trials.

## 2.3 Methods for analyzing spike-field coherence

In order to get an unbiased estimations of performance-related changes in spike-field coherence, subsets of correct trials, for each experiment, were selected such that pairs of correct and incorrect trials were as close as possible in time, leading to subsets containing in total 2402 trials (7 Sessions / 86 sites) for Monkey 1 and 1722 trials for Monkey 2 (5 Sessions / 66 sites). Then multitaper method was applied to get the spike-field coherence for each condition. To assess significant differences between trials with erroneous and correct responses, we permuted trials between conditions to construct  $H_0$  which predicts no performance-dependent difference.

### 2.3.1 Spectral analysis: Multitaper method

There are two broad classes of time series analysis: time domain techniques and frequency domain techniques. Spectral analysis is the prime example of a frequency domain technique and it has several advantages compared with time domain analysis. Firstly it is easier to detect subtle changes in signals when frequency domain estimator is computed. Secondly, due to non-stationary properties of neural signal, moving window estimate of spectra is less biased than that of time domain. Meanwhile it can give reasonably accurate confidence intervals.

A naive way to carry out nonparametric spectral analysis is Periodogram,



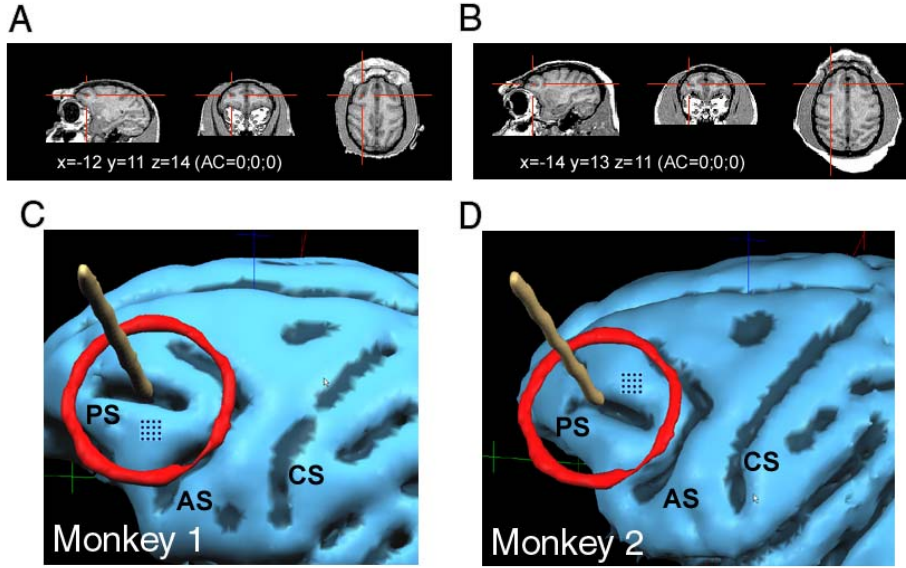


**Figure 2.2: MRI-based reconstruction of recording positions ([76]).** (A,B) 3D-MRI datasets for Monkey 1 and 2 which were used to guide implantation of recording chambers. The red crosses point to the principle sulcus of the left hemisphere very close to the actual positions of the chamber centers. The coordinates refer to the anterior commissure. (C,D) Lateral view on surface reconstructions of the frontal cortex of both monkeys. The labels denote principle sulcus (PS), arcuate sulcus (AS) and central sulcus (CS). The 3D-positions of the chambers were measured in a stereotaxic frame relative to the ear bars and the bone above the center of the left eye. The brown rods represent the axes of the actual chamber positions which came to be at  $x = -17, y = 7, z = 16$  for Monkey 1 and  $x = -17, y = 11, z = 13$  for Monkey 2. These coordinates indicate displacements of maximally 2 – 3 mm in the anterior-posterior and dorso-ventral directions relative to the planned target positions. The red circles represent the walls of the recording cylinders which were placed into the skull at 45 in the frontal plain and 10 in the transversal plain. The  $4 \times 4$  dot matrices illustrate the electrode-grids over ventral prefrontal cortex at the level of insertion through the surface of the cortex which was always in the ventral half of the chambers. ([76])

which takes the modulus squared of the Fourier transform of the data. This is the simplest example of a direct spectral estimator. The bias in the periodogram is negligible for some stationary processes. But if the dynamic range ( $10 \log_{10} \frac{\max_f S(f)}{\min_f S(f)}$ ,  $S(f)$  denotes the power spectrum of the signal) of the underlying process is high, the periodogram estimator is badly biased and could cause serious leakage([72]).

In order to lessen the bias in the periodogram, tapering method is usually applied. Tapering can reduce bias and minimize leakage. But only one taper is not sufficient to reduce the bias, since the sample size is effectively reduced after tapering. After smoothing across frequencies, this reduction results in a loss of information in the form of an increase in variance.

Multitaper was introduced in a seminal paper by Thomson [77] and involves the use of multiple orthogonal tapers. The basic idea of multitaper spectral estimation is to average the spectral estimates from several orthogonal tapers. The orthogonality of the tapers ensures that the estimates are uncorrelated for large samples. This makes it certain that multitaper is a scheme for recovering information. The choice for the independent tapers are discrete prolate spheroidal sequences (DPSS) or Slepian sequences, which are defined by the property that they are maximally localized in frequency.

Because of the non-stationary properties of the neural signals, a sliding-windowed multitaper analysis was applied (window length 200 ms, window shift 20 ms, 4 DPSS tapers with order 0 to 3). We computed the grand average spike-field coherence across all pairs (excluding signal pairs recorded at the same electrode) and all experiments for frequencies of interest (5 – 100 Hz, frequency steps 5 Hz). Later we focused on the frequency band 5 – 70 Hz, which covers alpha-, beta- and gamma-band signal.

### 2.3.2 Significance test: Permutation test

We tested the hypothesis that increases or decreases of spike-field coherence were performance related. To this end, we used the difference of spike-field coherence of correct and incorrect trials as the test statistic. Thus for each individual sliding window ( $t$ ), frequency of interest ( $f$ ), and pair of spike and local field potential signal ( $p$ ), the test static is chosen as

$$\Theta = \Theta_{t,f,p}^c - \Theta_{t,f,p}^i \quad (2.3.1)$$

where 'c' and 'i' stands for correct and incorrect trials respectively.

To evaluate the statistical significance of  $\Theta$ , we applied permutation test [75] to derive  $H_0$  distribution ( $H_0$ :  $\Theta$  is not performance related). The null hypothesis ( $H_0$ ) here means, if spike-field coherence is not modulated by different responses of the monkey,  $\Theta_{t,f,p}^c$  and  $\Theta_{t,f,p}^i$  should come from the same unknown distribution  $F$ . To generate the null hypothesis, permutation test gives us a simple and robust way, which is free of mathematical assumptions (see Fig. 2.3). After  $H_0$  is accessed by permutation test, the  $p$ -value could be estimated directly by comparing the original value  $\Theta$  and the value from null hypothesis  $\Theta^*$ . In other words,  $p$ -value could be obtained by computing  $p_l$  ( $\Theta < \Theta^*$ ) for left sided test and  $p_r$  ( $\Theta > \Theta^*$ ) for right sided test(test level 1.5%). Based on these  $p$ -value, we computed for each frequency bin and sliding window the percentage of pairs per session that showed a significant increase in spike-field coherence for correct or incorrect responses. To estimate the expected probability of pairs with significant modulation in a given frequency band (band 1: 5 – 20 Hz and band 2: 25 – 70 Hz), the results were averaged across sessions and across the respective frequencies of the same band.

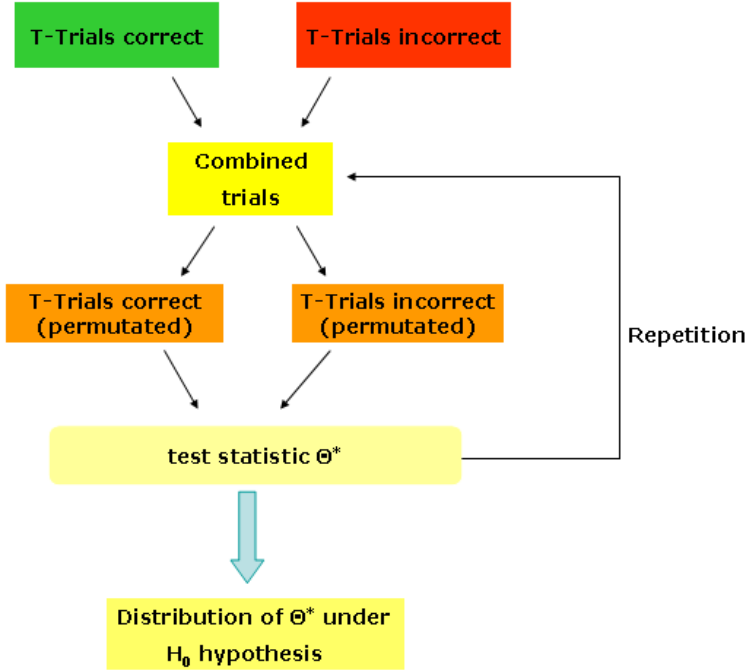


**Figure 2.3: Basic principles of the permutation test.** The basic idea of permutation test is that samples from permuted trial-set forms  $H_0$ . To estimate the distribution  $H_0$ , permutation is resampling the combined trial-sets. Based on the set of all potentially existing permuted samples,  $H_0$  can be approximated by and ideal estimated.

### 2.3.3 $\lambda$ -maps

To allow for variability in the timing and frequencies of states or processes related to behavioral performance across sessions and subjects, time-frequency maps of the results were smoothed with a Gaussian kernel ( $\sigma_t = 200$  ms /  $\sigma_f = 5$  Hz). Smoothed time-frequency maps are referred to as  $\lambda$ -maps, where  $\lambda_c$  describes the percentage of pairs with a significant increase in spike-field coherence for correct trials, while  $\lambda_i$  describes that for incorrect trials. Due to the fact that  $\lambda_c$  describes the percentage of sites with a significant

difference between correct and incorrect trials, an increase in  $\lambda_c$  does not imply a decrease in  $\lambda_i$  for incorrect response. Two different subpopulations could still behave in an opposite fashion. To assess task-related modulation of  $\lambda$ , we derived baseline-corrected modulations by computing the z-score that compares  $\lambda$  during task execution between 0 second and 4.5 second to the mean value and the variability during the pre-sample period ( $-0.5$  to  $0$  second). In other words, the z-score is defined as

$$z \equiv \frac{\lambda - E\{\lambda_b\}}{\sigma_{\lambda_b}} \quad (2.3.2)$$

where  $\lambda_b$  stands for the  $\lambda$  value of the baseline. Frequencies were treated separately to allow for frequency band specific pre-sample difference like attention related increases.

## 2.4 Results of experimental data

After applying multitaper method as described above, we got the spike-field coherence of correct and incorrect responses respectively (Fig. 2.4).

From the figures of the spectra, we cannot clearly distinguish the results from correct and incorrect responses. Since the spike signal gives a broad-band spectra in frequency domain, the modulations of the spike-field coherence due to different performance is hardly to see directly from the figure. Thus, to evaluate the significance of these spectra becomes the key point of the study. Since the permutation test could give us the nonparametric evaluation of the  $p$  value, we pooled the original dataset and applied permutation test.

When permutation test was applied to the experimental data, we chose the permutation replications to 100 and the test level was set as 1.5%. It was shown ([76]) before that the  $B_{perm} = 100$  gives enough confidence in the empirical distribution to be used for a hypothesis test based on a testlevel of 1.5%. To further investigate whether it is still valid in our case, permutation

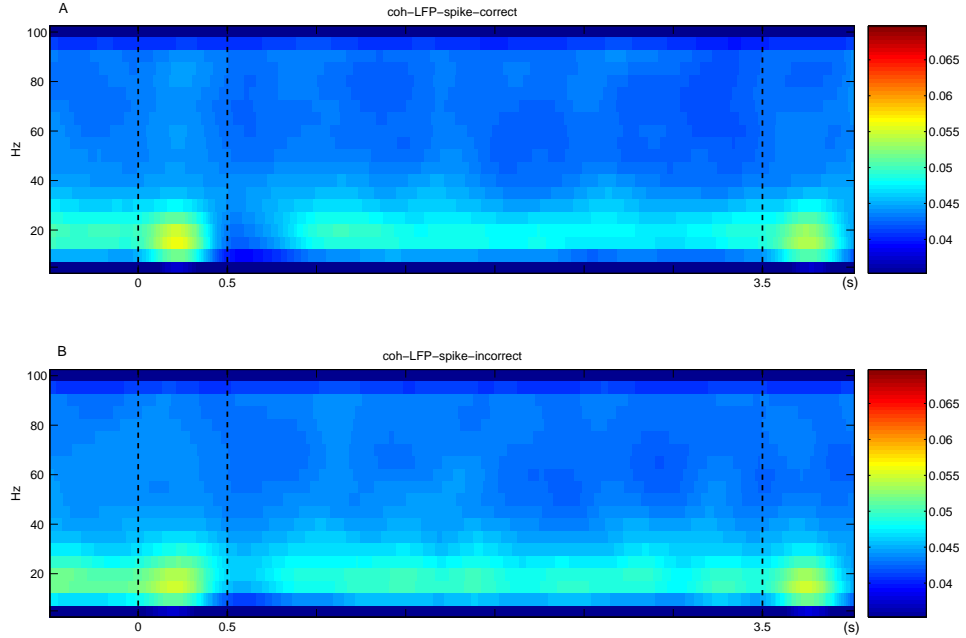


**Figure 2.4: Grand average time-frequency ('TF') plots for spike-field coherence.** (A, B) TF plots of grand average spike-field coherence of all simultaneously recorded signals from two monkeys recorded in 12 sessions with a total of 4124 trials, from 146 sites and 1593 pairs. (A) Grand average spike-field coherence for trials with correct responses; (B) Grand average spike-field coherence for trials with incorrect responses.

test was applied on session 5122 to testify the assumption. We chose the permutation replications as 100 and 1000 respectively and applied the same methods to get the  $\lambda$ -map (Fig. 2.5). From the figure we could see that, although the left-hand plots are not exactly the same with the right-hand ones, the stronger effect occurs at the same period (correct: 0.5 second, incorrect: 1.5 second) and the effect of increase in spike-field coherence is in the same range (0.03 – 0.035), which indicates that in this case 100 replications with significance level 1.5% is good enough for us to evaluate the significance of the

spectrum of spike-field coherence.

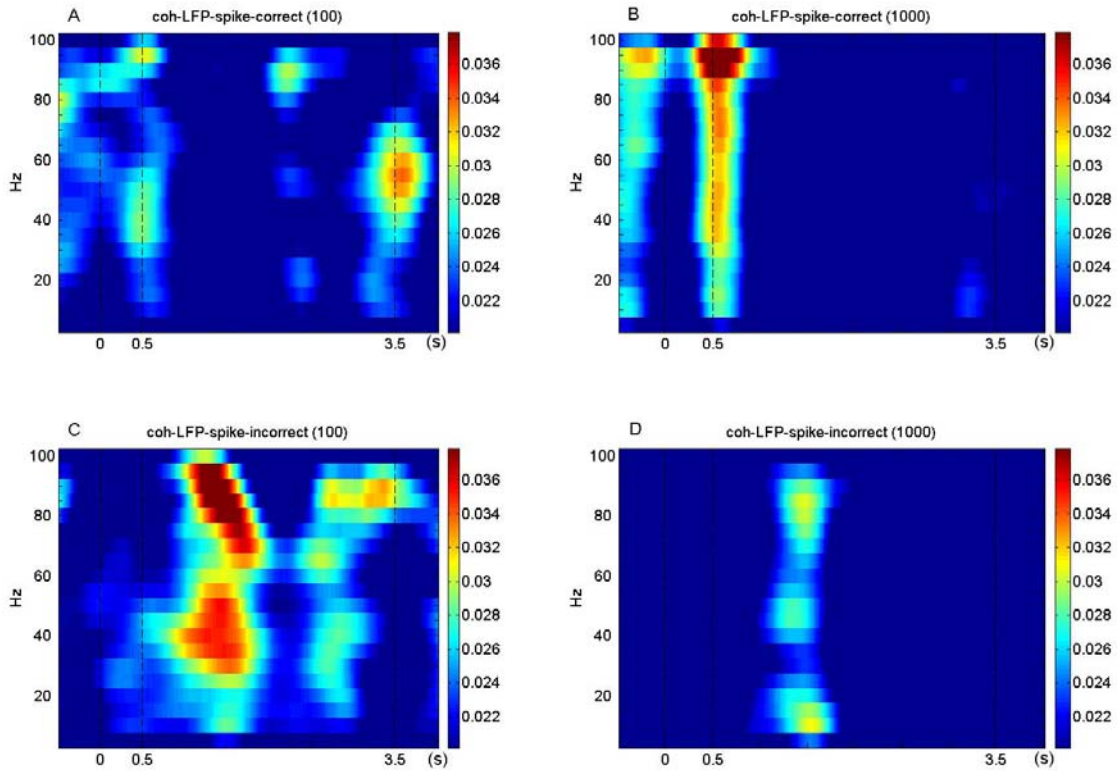


**Figure 2.5:  $\lambda$ -map of Session 5122 with different permutation replications.** (A)  $\lambda$ -map with 100 replications for correct trial-set. (B)  $\lambda$ -map with 1000 replications for correct trial-set. (C)  $\lambda$ -map with 100 replications for incorrect trial-set. (D)  $\lambda$ -map with 1000 replications for incorrect trial-set.

$\lambda$ -maps of spike-field coherence revealed values ranging from 0.5% (significance threshold, see Fig. 2.6) to 3.5% for the different frequency bands and different periods of the task. As shown in Fig. 2.6, for the correct trials, there are strong modulations in gamma-band oscillation during the stimulus and delay periods. Just after the stimulus and during the test period, there is a significant increase in spike-field coherence in beta- and gamma-band for correct trials. This shows that when the monkey had a correct response, the coding of the stimulus and the maintenance of the information are mainly involved in gamma-band

oscillation.

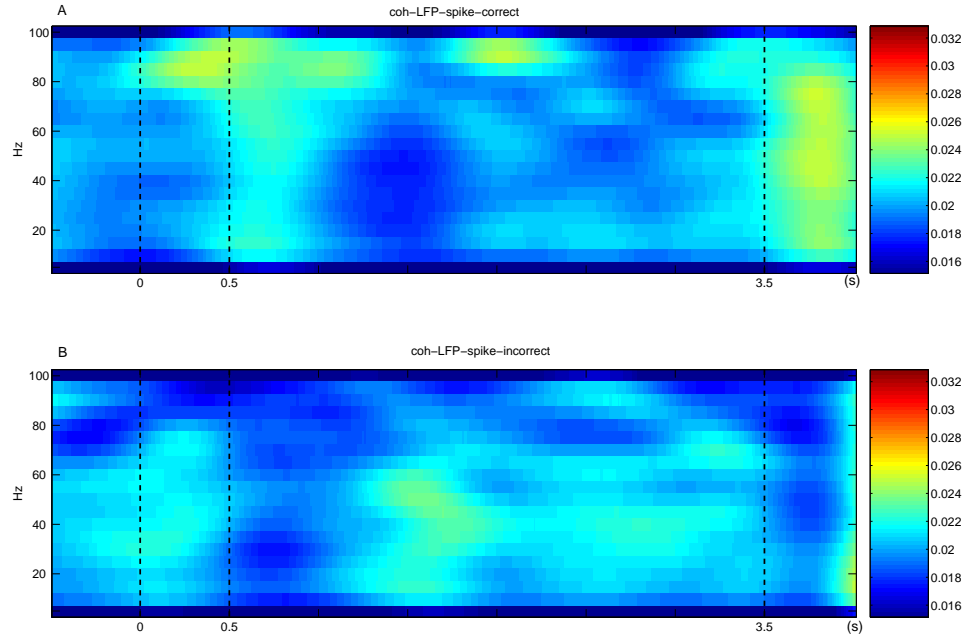


**Figure 2.6: Performance-dependent increase of  $\gamma$ -oscillations in spike-field coherence in prefrontal area.** (A) Time-frequency  $\lambda_c$ -maps. It provides the percentage of sites/pairs with significant increases of spike-field coherence in trials with correct responses. (B) Time-frequency  $\lambda_f$ -maps provides the results of incorrect response.

In order to rule out spontaneous fluctuations as the cause for these comparatively small changes, we performed a z-transform with respect to variability during the pre-stimulus baseline. The time course of z-transformed spike-field coherence was found to be modulated in two frequency bands (Fig. 2.7) and shows remarkable differences for trials with correct and incorrect responses (compare Fig. 2.7 a and b). The most prominent modulation was observed for the gamma frequency band (25–70 Hz) in correct trials ( $\lambda_c$ ), which yielded z-scores between  $-15$  and more than  $40$ . In contrast, the maximal modulation



of  $\lambda_i$  only reached values that were about 4 times smaller than  $\lambda_c$ . Interestingly, the lower frequencies (5 – 20 Hz) comprising the classical theta, alpha, and beta range exhibited a task-related modulation during trials with correct responses, which differed from the modulation in the gamma band in two respects: it occurred earlier in response to the sample stimuli and did not reflect the processing of test stimuli at all. This demonstrates that the observed modulations, even though they are rather small, are tightly correlated with the task and the monkey’s performance.

## 2.5 Simulated-data model and method calibration

As shown previously [71], there is a lower bound beyond which additional smoothing of multitapered spectra does not further decrease the variance. This lower bound is approximately reached when the degrees of freedom roughly equal twice the total number of spikes in all trials. The degree of freedom of the multitaper method is given by:  $\nu_0 \cong 2T_r K_t$  with  $T_r$  representing the number of trials and  $K_t$  the number of tapers. Since the expected total number of spikes is given by the product of the spike rate, the number of trials, and the length of the sliding window ( $l$ ), the lower bound  $r_l$  of the spike rate is:  $r_l \cong K_t/l$ , which amounts to  $r_l = 20$  spikes/sec (spikes/second) for  $K_t = 4$  and  $l = 0.2$  s as used for analyzing the experimental data.

Since recordings in prefrontal cortex are characterized by spike rates in the range of a few spikes per second, which is below the critical  $r_0$ , estimates of spike-field coherence for individual pairs might yield large variability. Nevertheless, the experimental results assessed by  $\lambda$  are based on the average of more than 1500 estimates for performance-related differences in spike-field coherence. Thus, to judge the reliability of  $\lambda$ , we generated simulated data

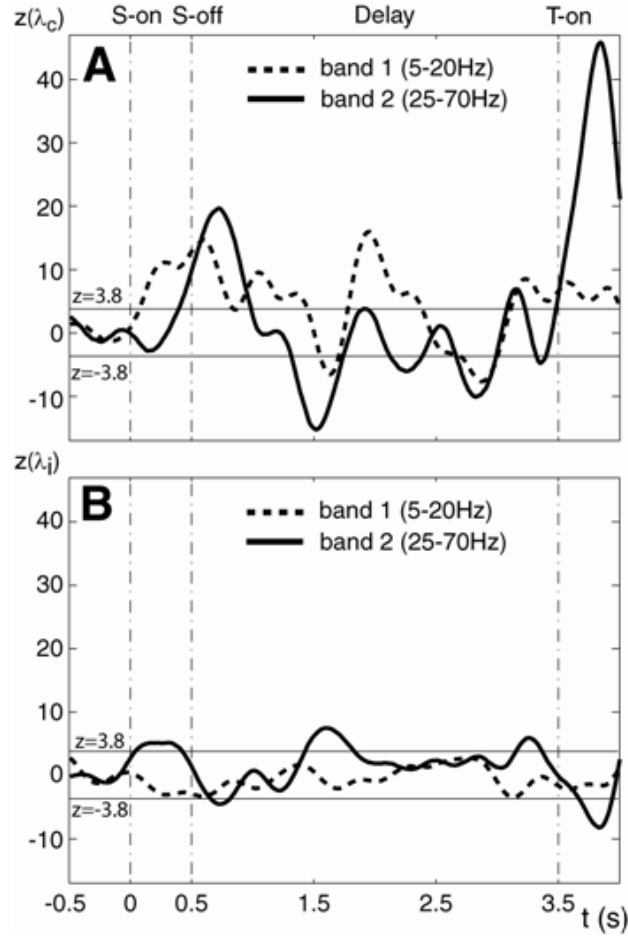


**Figure 2.7: Time course of significance for spike-field coherence with respect to the pre-sample period.** (a) Z-score of average  $\lambda_c$ , which represents the percentage of pairs with robust increases of spike-field coherence during correct trials. The dotted line represents the average  $\lambda_c$  value in the frequency band from 5 to 20 Hz, while the solid line represents the average  $\lambda_c$  value in the frequency band from 25 to 70 Hz. (b) Corresponding z-score of average  $\lambda_i$ , for increases of spike-field coherence during incorrect trials. Z-values larger than 3.76 and smaller than  $-3.76$  (Bonferroni corrected test level for 1.5% and 170 sliding windows) indicate significant task-related increases and decreases at a 5% significance level, respectively.

comprised of exactly the same data structure, i.e. the same number of experiments, trials, and pairs of local field potentials and spike signals, and we applied the same analysis as on the experimental data.

To model local field potential signals, we simulated a sinusoidal oscillation with additive white noise that had half the amplitude of the oscillation (Fig. 2.8 a). That is to say, the local field potential signal was chosen as

$$s(t) = A * \sin(2\pi f_0 t) + \frac{A}{2} * \zeta(t), \quad (2.5.1)$$

where  $A$  stands for the amplitude of the local field potential signal,  $f_0$  stands for the central frequency of the sinusoidal oscillation,  $\zeta(t)$  denotes white noise with expectation  $E\{\zeta(t)\} = 0$ . To model effects in the low- and high-frequency bands, we generated simulated local field potentials containing frequencies (12.5 Hz and 50 Hz) at the centers of the two frequency bands analyzed in the experimental data (see Fig. 2.7). Spike data were modeled as Poisson processes. In order to compare the results for simulated and experimental data, we modeled two classes of spike data analogous to trials with correct and incorrect responses. Spike data corresponding to incorrect trials were modeled by a homogenous Poisson process with a spike rate  $r_0 = 5$  spikes/sec, which is comparable to the lower bound of experimental spike rate. Spike data corresponding to correct trials were modeled by an inhomogeneous Poisson process based on a spike-rate profile with periods of length  $w$  and rate increasing from  $r_0$  to  $r_1 = 25$  spikes/sec, which then were phase-locked to the local field potentials. To further investigate the nature of the processes underlying spike-field coherence, we modified the temporal correlation of the model and compared the results based on the simulated data and the actual recordings. Spikes induced during these short epochs were phase-locked to the local field potential oscillations if  $w$  was small compared to the period length ( $T$ ) of the oscillation (Fig. 2.8 b). Thus, modifying  $w$  enabled us to manipulate spike-field coherence based on the modulation of the phase-precision.

Given different sinuous oscillations, the same  $w$  value could lead to different phase relations between local field potentials and spike signals. For instance, if the underlying frequency of sinuous oscillation is chosen as 12.5 Hz, the corresponding period of the simulated local field potential is 80 ms. When  $w$  is 2 ms for spike signals, the phase relation between these two signals is

$$\phi = w/T * 2\pi = 2/80 * 2\pi = 0.05\pi \quad (2.5.2)$$

Using the same  $w$  value, if the central frequency of sinuous oscillation is 50 Hz, the phase relation between simulated spikes and local field potentials is  $0.2\pi$  (Fig. 2.8 c).

To model different strengths of synchronization rather than the phase-precision, we changed the maximal rate modulation  $r_1$  from 25 spikes/sec to 45 spikes/sec. Hence, we controlled two parameters that could cause changes of spike-field coherence in the simulated data: first, the period width  $w$  that modifies the phase-precision between local field potentials and spike signal and second, the difference in  $r_1$  to change the strength of synchronization.

The analysis of the simulated data revealed maximal  $\lambda$  values of 40% for  $r_1 = 25$  and 55% for  $r_1 = 45$  in the low frequency band 1, which means that the corresponding experimental data with a maximum of 3.5% were far less well locked, while maximum  $\lambda$  values in the high frequency band 2 amounted to 2.7% and were equal for both  $r_1 = 25$  and  $r_1 = 45$ . Increasing  $w$  to values compatible with  $T$  diminished  $\lambda$  to values of about 0.5% for all models (Fig. 2.8 e, g). Nevertheless, the relation of  $T$ ,  $w$ , and the modulation of  $r_1$  interact (Fig. 2.8 d-g) as the decreases of test power were not monotonic with changes of  $w$ . Only for the smaller  $r_1$  values and larger values of  $w$  does test power decrease monotonically at high frequencies. At lower frequencies, the test power reached its maximum at intermediate values of  $w$  (Fig. 2.8 e). The reason for this is that longer windows, which are small compared to  $T$ , contain more spikes and are therefore more precisely locked to the local field

potentials. The average  $\lambda$  and its standard error in the case of  $H_0$  amount to 0.5% and 0.05%, respectively. The average  $\lambda$  is below the test level (1.5%), which indicates a conservative significance. The variability of  $\lambda$  is very low, due to the large number of pairs used. Hence,  $\lambda$  values larger than 0.6 cannot be explained by chance ( $mean + 2 * std$ ). This demonstrates that our new approach is a reliable and sensitive method to detect differences in spike-field coherence, even at low spike rates.

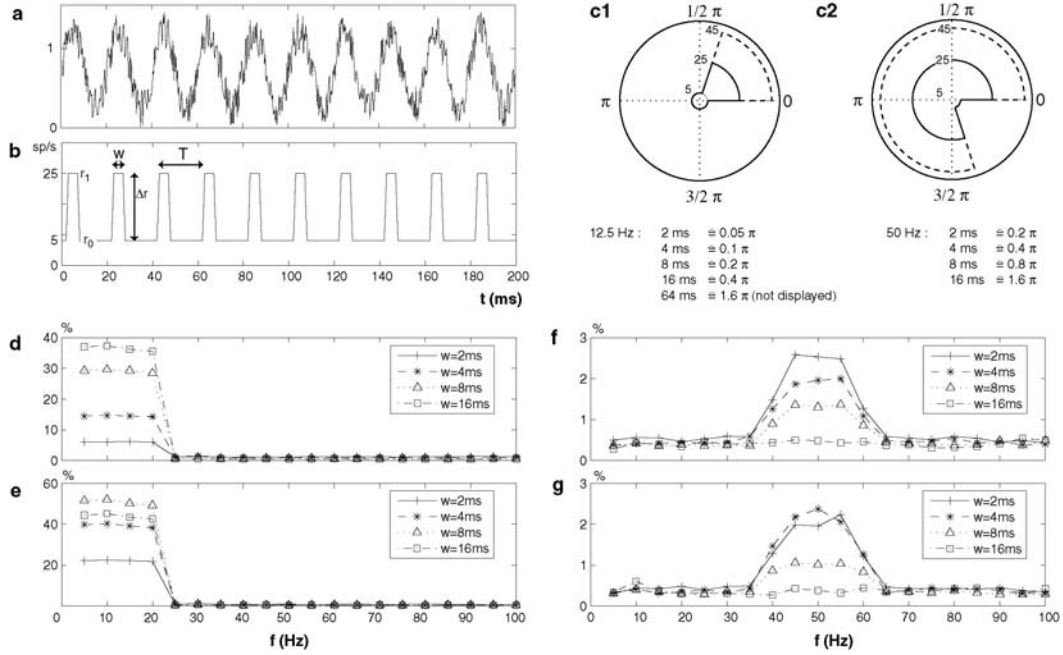


**Figure 2.8: Test power of simulated data.** (a) Local field potential signal composed of a sinusoidal oscillation and additive white noise with amplitude half of the oscillation. (b) The rate profile of spike trains has a strong phase relation with the local field potential signal. (c) Polar plots of the rate profile for  $f_0 = 50$  Hz and  $w = 4$  ms in C1 and  $w = 16$  ms in C2. (d-g) Test power for spike-field coherence between local field potential and spike signals. (d:  $f_0 = 12.5$  Hz,  $r_1 = 25$  spikes/sec (spikes/second); e:  $f_0 = 12.5$  Hz,  $r_1 = 45$  spikes/sec; f:  $f_0 = 50$  Hz,  $r_1 = 25$  spikes/sec; g:  $f_0 = 50$  Hz,  $r_1 = 45$  spikes/sec)

## 2.6 Discussion

The value of  $\lambda$  for spike-field coherence performance-related differences in the high-frequency band (25 – 70 Hz) amounted to compatible values for the experimental and simulated data: 3.5% and 2.7%, respectively. The same is true for the average baseline value of  $\lambda$  and its variability in the experimental and simulated data. Therefore, the analysis of both datasets revealed the same maximal relative modulation of  $\lambda$  expressed as a change in z-score of about 40. This demonstrates that even though the variability of individual spike-field coherence estimates might be rather large, assessments of performance-related differences of  $\lambda$  based on a large number of estimates is highly reliable. Quantitative comparison of the two types of simulated data, the one modeling phase-precision and the one modeling the strength of synchronization, indicates that experimental results in the high-frequency band are most likely based on precisely phase-locked spikes that have a low probability of occurrence. Given the results of the simulated-data analysis, spikes must be locked with a precision of less than 2 ms to local field potential oscillations at 50 Hz (phase-precision:  $0.2\pi$ ) to reach  $\lambda$  values close to the maximal values (3.5%) observed in the experimental results. However, given the rather short period ( $w = 2$  ms), an oscillation frequency of 50 Hz, and a rate  $r_1 = 25$  spikes/sec, we expect 0.5 phase-locked spikes per sliding window. This illustrates, first, that the method is very sensitive and second, that differences in spike-field coherence due to behavioral performance might be based on rather few synchronous events in prefrontal cortex, which cannot be explained by chance.

## 2.7 Summary

Although differences among behavioral conditions appear to be based on a rather few instances of phase-locked spikes, the task-related effects on spike-

field coherence are highly reliable and cannot be explained by chance, as the comparison of experimental results and the results from simulated-data analysis shows. The differential locking of prefrontal neuron populations with two different frequency bands in their input signals suggests that neuronal activity underlying short-term memory in prefrontal cortex transiently engages cortical circuits on different spatial scales, probably in order to coordinate distributed processes. Moreover, the precise locking between spike and local field potential oscillations during behavioral transitions elucidates that transient coordination of local and more global circuits might be necessary during memory encoding and retrieval.

# Chapter 3

## Bi- and multi-variate spike train analysis

### 3.1 Introduction

To test the importance of synchronous neuronal firing according to information processing in the brain, one has to investigate if synchronous firing and its strength are correlated to the state of the neuronal system, or the behavior and the task of the experimental subject ([80], [81], [82]). This requires a tool that can compare the strength of the synchronous firing across different conditions ('factors'), while it corrects at the same time for other features of neuronal firing such as spike rate modulation or the auto structure of the spike trains that might co-occur with synchronous firing. Previously developed method NeuroXidence [76, 78, 79] is for uni-variate case and therefore optimized to detect synchronous firing beyond that expected by chance reliably, but do not allow to compare the strength across factors, or suitable for comparing different factors and was not robust against features that were discussed to induce false positives. In this chapter we present a bi- and multivariate extension of NeuroXidence. This extension allows comparing the amount of synchronous



firing between different factors for the same spiking pattern. The new extension is robust against rate changes of individual neurons and against rate co-variation of groups of neurons. It considers the full auto structure as well as trial by trial variability. The basic idea of the bi- and multivariate extension is that one first determines the frequency of a certain joint-spike event (JSE) for each trial and each factor of the experiment. Next, surrogate data is generated such that each surrogate spike train is identical to the original data but any fine temporal cross structure between simultaneously recorded spike trains is destroyed by jittering the whole spike train by a random amount time step. To this end we define two timescales. The first time scale  $\tau_c$  defines the expected precision of JSE and it is usually in the order of a few milliseconds. The second time scale is  $\tau_r$ , which is  $\eta$  times slower than  $\tau_c$ , and it defines the lower bound of rate modulation. This surrogate data serves the estimation of the frequency of chance JSE under the  $H_0$  assumption that neurons are not coupled in a fine temporal timescale. Hence, the frequencies of JSE occurring in the surrogate dataset are used to correct the frequency of JSE in the original dataset. To this end the difference is computed between the original and the surrogate dataset for each trial and each factor. Differences due to different factors are detected based on bi-variate mean or median tests (t-test, and Mann-Whitnes U test) or by ANOVA test in the multivariate case. Hence the result of  $p$ -value tells us how likely it is to explain modulations of synchronous firing on the time scale  $\tau_c$  across factors by chance.

## 3.2 Method

We used the same way of detection of JSEs as shown in the previous paper [78, 79]. First, we defined two parameters:  $\tau_c$  and  $\tau_r$ .  $\tau_c$  is the timescale of synchronous firing which ranges between 1 and 10 ms; while  $\tau_r$  is distinguishably slower than  $\tau_c$ , with a factor  $\eta$  introduced as the ratio between these two

timescales  $\tau_r = \eta * \tau_c$ , which ranges from 2 to 5. Then we generated surrogate data by jittering the original individual spike train within slow timescale  $\tau_r$ , which destroys the fine temporal cross-structure less than  $\tau_r$  but keeps the auto-structure and other features. Thus for a particular JS-pattern  $k$ , trial  $t$  and condition  $\xi$ , the difference between original and surrogate dataset for each condition could be computed as

$$\overline{\Delta}f_{t,\xi}^k = \frac{1}{S} \sum_{s=1}^S \Delta f_{t,\xi,s}^k = f_{t,\xi}^k(org) - \frac{1}{S} \sum_{s=1}^S f_{t,\xi,s}^k(sur), \quad (3.2.1)$$

where  $f_{t,\xi}^k(org) \in N_0$ ,  $\overline{\Delta}f_{t,\xi}^k \in Q$ , for trial  $t = 1, 2, \dots, T_r$  and JS-pattern  $k = 1, 2, \dots, K$ , surrogate  $s = 1, 2, \dots, S$  and condition  $\xi = 1, 2, \dots, M$ .

In bi-variate case, we chose the difference of JSEs between two conditions as the test statistic. In other words, for each trial  $t$  and each JS-pattern  $k$ , we compute the difference  $\overline{\Delta}\Theta_t^k = \overline{\Delta}f_{t,1}^k - \overline{\Delta}f_{t,2}^k$ , where  $\overline{\Delta}f_{t,1}^k$  and  $\overline{\Delta}f_{t,2}^k$  are the average differences between original and surrogate dataset for condition 1 and condition 2 respectively. If  $\overline{\Delta}\Theta_t^k$  is larger than zero, it means an excess of JSEs for one particular JS-pattern  $k$  in condition 1; while  $\overline{\Delta}\Theta_t^k$  is smaller than zero, it means an excess of JSEs in condition 2. The difference  $\overline{\Delta}\Theta_t^k$  for one particular JS-pattern  $k$  from all trials form the set  $\overline{\Delta}\Theta^k$ :

$$\overline{\Delta}\Theta^k = \{\overline{\Delta}\Theta_1^k, \overline{\Delta}\Theta_2^k, \dots, \overline{\Delta}\Theta_{T_r}^k\}. \quad (3.2.2)$$

We applied mean test (t-test) and median test (Mann-Whitnes U test) to set  $\overline{\Delta}\Theta^k$  to check whether the excess or lacking of JSEs between two conditions is significant and consistent across trials.

As for multivariate case, for each condition  $\xi$  and each particular JS-pattern  $k$  from all trials  $t = 1, 2, \dots, T_r$ , the differences  $\overline{\Delta}f_{t,\xi}^k$  form the set  $\overline{\Delta}F_\xi^k$ :

$$\overline{\Delta}F_\xi^k = \{\overline{\Delta}f_{1,\xi}^k, \overline{\Delta}f_{2,\xi}^k, \dots, \overline{\Delta}f_{T_r,\xi}^k\}. \quad (3.2.3)$$

where condition  $\xi = 1, 2, \dots, M$ . Thus the differences from all conditions form the set

$$\overline{\Delta}\Theta^k = \{\overline{\Delta}F_1^k, \overline{\Delta}F_2^k, \dots, \overline{\Delta}F_M^k\}. \quad (3.2.4)$$

ANOVA was then applied to the set of differences  $\overline{\Delta\Theta}^k$  to check whether one of  $\overline{\Delta F}_\xi^k$  is significantly different from others.

### 3.3 Method calibration (Part I)

First, we carry out method calibration for bivariate case. As described above, we compared  $\overline{\Delta\Theta}^k$  for two simulated datasets to examine the detection of JSEs of NeuroXidence method.

#### 3.3.1 False positives for two stationary processes

We generated two simulated datasets to stand for two conditions, and each of them has 8 neurons and each spike train is generated by independent and stationary Poisson processes. Here we used two scenarios to generate Poisson spike trains for both conditions.

**Scenario one:** we set the mean spike rates of two simulated datasets to the same value and changed them together, then we applied NeuroXidence to check whether the JSEs from two simulated datasets were significantly different.

**Scenario two:** we set the mean rate of one simulated dataset to a fixed value (for example 15 spikes/sec (spikes/second)), and changed the mean rate of the other simulated dataset. NeuroXidence was applied to check whether JSEs from one condition is significantly different from the other.

The standard set of parameters for scenario one was defined by 50 trials ( $T_r$ ), mean spike rate of 15 spikes/sec ( $r$ ), 20 surrogates samples ( $S$ ), and  $\eta$  equals 5. From the standard parameter set, 8 different combinations of parameters were derived by varying the number of trials ( $T_r = 20, 50, 100$ ) and the mean spiking rate ( $r_1 = r_2 = 7, 10, 30, 60, 90$  spikes/sec). And the standard set of parameters for scenario two was defined by 50 trials ( $T_r$ ), mean spike rate of

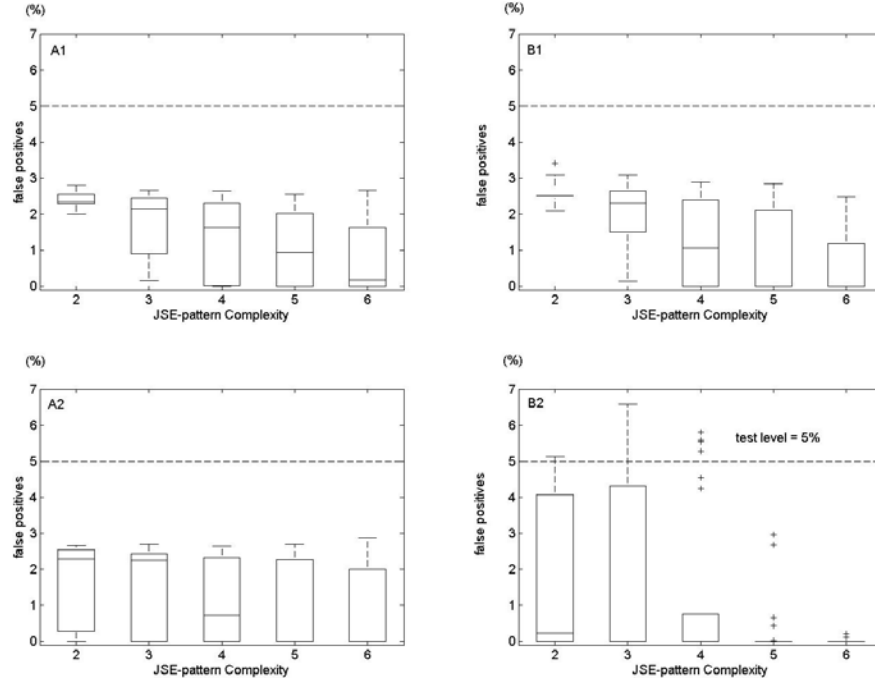


**Figure 3.1: Percentage of false positives estimate by NeuroXidence used to detect joint-spike patterns of complexity 2 to 6 for bivariate cases with test level 5%.** Two simulated datasets were generated by independent and homogenous Poisson processes and NeuroXidence was used to estimate joint-spike events (JSEs) based on 200 independent realizations for each simulated data model. The difference between these two estimates is taken as the test statistic to evaluate the false-positive rate. The standard parameter set is as follows: trial= 50, spike-rate= 15 spikes/sec (spikes/second), and  $\eta = 5$ . **(A1)** and **(A2)**: mean spike rates of two conditions change together ( $r_1 = r_2 = 7, 10, 30, 60, 90$  spikes/sec), after applying NeuroXidence to detect the joint-spike patterns, we use t-test **(A1)** and Mann-Whitnes U test **(A2)** respectively, with variation the number of trials ( $T_r = 20, 50, 100$ ). Here we set surrogate to 20. **(B1)** and **(B2)**: we set mean spike rate of condition one to 15, and that of condition two changes from 7 to 90 ( $r_1 = 15, r_2 = 7, 10, 30, 60, 90$  spikes/sec), then applied NeuroXidence and used t-test **(B1)** and Mann-Whitnes U test **(B2)** to evaluate the false positive rates with variation the number of trials ( $T_r = 20, 50, 100$ ). Here we set surrogate to 1.

15 spikes/sec ( $r$ ), 1 surrogate samples ( $S$ ), and  $\eta$  equals 5. From the standard parameter set, 8 different combinations of parameters were derived by varying the number of trials ( $T_r = 20, 50, 100$ ) and the mean spiking rate ( $r_1 = 15, r_2 = 7, 10, 30, 60, 90$  spikes/sec). We applied NeuroXidence to each simulated dataset using a sliding window with duration of  $l = 200$  ms. In total, 8 different simulated data models were used to get the false-positive-rate for five JS-patterns of complexity 2 – 6. None of the results from any of the parameter sets exceeded the chance-level, for either test-level 5% (Fig. 3.1) or 1% (Fig. 3.2). This shows that NeuroXidence detects JSEs in a conservative way for bivariate case.

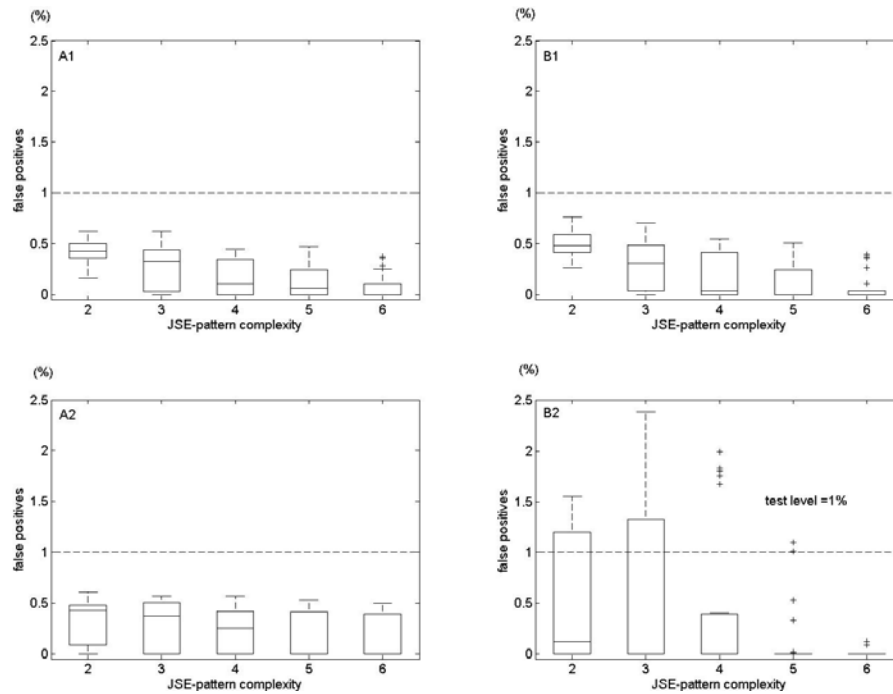


**Figure 3.2: Percentage of false positives estimate by NeuroXidence used to detect joint-spike patterns of complexity 2 to 6 for bivariate cases with test level 1%. The notation is the same as Fig 3.1.**

### 3.3.2 Test-power for stationary process

To access the test power of NeuroXidence for bivariate case, one simulated dataset was modeled as single-interaction process based on Poisson process, while the other was generated by independent and homogenous Poisson process. Each dataset contains 8 simultaneous spike trains. For single-interaction process, correlated spike trains were characterized by a background rate, which corresponds to the independent spiking of neurons, and by a JSE rate, defining the expected frequency of the JS-pattern of interest beyond that of the other condition.

The standard parameter set is chosen as 50 trials ( $T_r$ ), the background spike rate of 15 spikes/sec ( $r$ ), 20 surrogates numbers ( $S$ ), and  $\eta$  equals 5. Eleven parameter sets were used to study how the test-power of NeuroXidence is affected by the number of trials ( $T_r = 20, 50, 100$ ), the background spike rate ( $r_1 = r_2 = 10, 15, 30, 60, 90$  spikes/sec), and the number of surrogates ( $S = 1, 20, 50$ ). Based on 11 simulated datasets, the test-power was derived from five JS-patterns of complexity 2 – 6. The test-level was set to 5%. From Fig. 3.3, we could see that increasing the number of trials would lead to an increase of test-power. Given the same frequency of excess JSEs, higher complexity patterns are more likely to be detected than lower complexity patterns. With increasing the background rate, one need more JSEs to get the same test power. However, for higher complexity patterns, this effect is reduced. As for lower complexity patterns, larger number of surrogates ( $S$ ) is required, for example,  $S = 20$  is good enough for the test power. While for higher complexity patterns, number of surrogates doesn't show an important effect on the test power. Thus one could choose  $S = 1$  for higher complexity patterns.

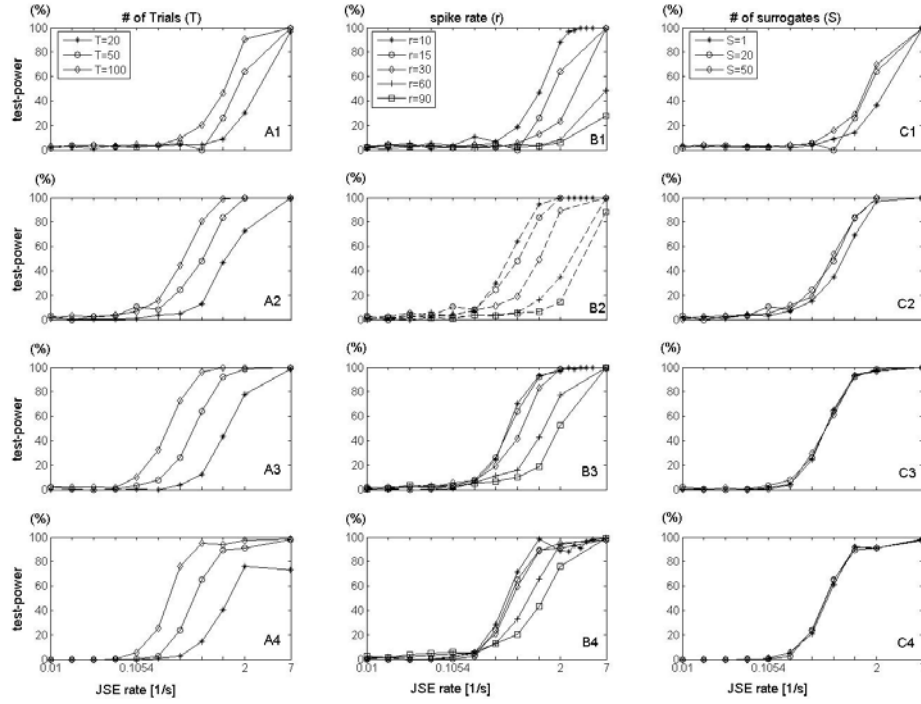


**Figure 3.3: Test power of NeuroXidence in relation to the number of trials ( $T_r$ ), spike rate( $r$ ) and number of surrogates ( $S$ ) in bi-variate case.** One simulated dataset was modeled as single-interaction process based on Poisson process, while other was generated by independent and homogenous Poisson process. NeuroXidence was used to estimate the JSEs for each simulated dataset. The test statistic is chosen as the difference between different frequencies of JSE for each simulated data model. Subfigures plot the test-power of NeuroXidence as a function of the frequency of JSEs beyond chance level. Rows 1 – 4 show the test-power dependencies on the complexities of the analyzed joint-spike pattern ranging from 2 to 5. **(A1-A4)** variations in the number of trials  $T_r$ , **(B1-B4)** variations in the spike rate  $r$ , **(C1-C4)** variations in the number of surrogates  $S$  from standard parameter set ( $T_r = 50$ ,  $r = 15$  spikes/sec,  $S = 20$ ,  $\eta = 5$ ,  $l = 200$ ms).

### 3.3.3 Sub- and Supra-patterns of induced JS-patterns

Sub-patterns and supra-patterns are defined in the way as shown in the previous paper [78, 79]. A single-interaction process and an independent and homogenous Poisson process were used to generate two simulated datasets. Each dataset contained 50 trials of 8 simultaneous spike trains.

To study the test-power of sub-patterns and supra-patterns of two different processes, we applied a statistical evaluation of the frequency of occurrence of any potentially existing JS-patterns in four complexities of the mother-patterns, which are the JS-patterns induced by the single-interaction process. Any JS-pattern of complexity higher than 2 includes sub-patterns that are expected to be detected because of existence of mother-pattern. If sub-patterns are only induced by one mother-process and not by additional correlations with orders equal to or smaller than the complexity of the sub-patterns, the test-power is expected to decrease with the decreasing complexity of the sub-pattern. Supra-patterns are composed of the mother-pattern itself and spikes from additional neurons, which are by chance coinciding with the mother-pattern. The maximal frequency of a supra-pattern is bound by the maximal frequency of any sub-pattern, including the induced mother-pattern. Since the additional spikes are coinciding by chance, the frequency of the supra-pattern occurrence is expected to be smaller than that for the mother-pattern. Thus, as long the excess frequency of the mother-pattern is not so high, the test-power of the supra-pattern is expected to be substantially reduced in relation to the mother-pattern (Fig. 3.4).

### 3.3.4 False Positives for a non-stationary process

By generating datasets from non-stationary processes, we derived the percentage of false positives of JSEs detected by NeuroXidence. Each of the two simulated datasets comprised 18 simultaneous units and 50 trials, which were



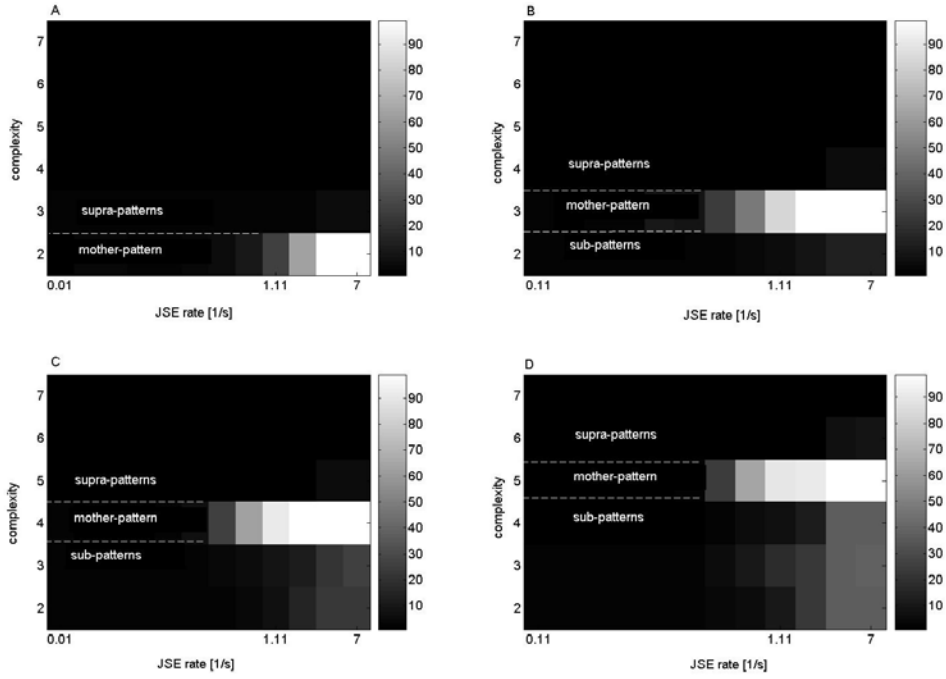


**Figure 3.4: Test-power of NeuroXidence for an induced mother-pattern and its supra-patterns and sub-patterns.**

Two sets of simulated data were generated as two processes described before. Each sub-figure shows the grey-coded test-power of a certain mother-pattern, all sub-patterns of lower complexities, and all supra-patterns of higher complexities. The excess rate of JSEs beyond the chance-level, which corresponds to the mother-pattern, is given on the x-axis. The data used to derive the test-power consisted of 50 trials of 8 spike trains. A spike rate  $r = 15$  spikes/sec,  $S = 20$  surrogates, and  $\eta = 5$  were used by NeuroXidence for deriving the statistical significance. **A-D** shows the variations of mother-pattern of complexity 2 to 5.

based on 12 periods, each lasts 2 seconds (Fig. 3.5). The simulated datasets contained features that are often observed in real datasets, such as low rates (Period 3, 4), rate modulation (Periods 5-10), and latency co-variation of rate responses across neurons (Periods 8, 10).

NeuroXidence was applied to each dataset in a sliding window of length 800

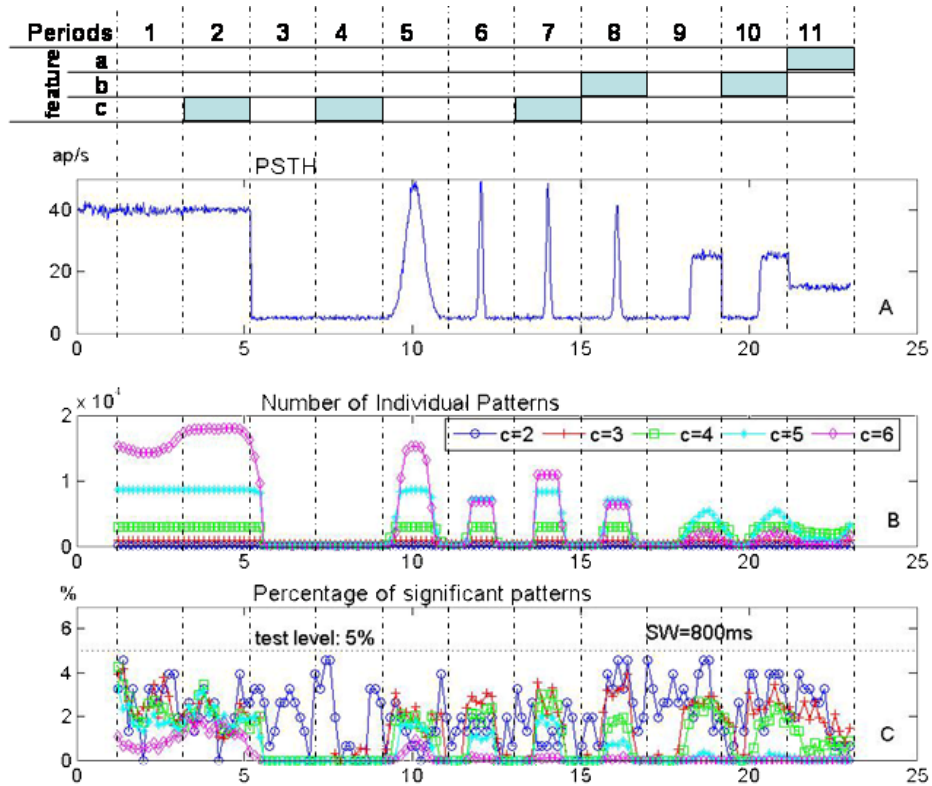


**Figure 3.5: False positives for non-stationary processes evaluated by NeuroXidence.** Generated two simulated datasets and each consisted of 50 trials of 18 'simultaneous' spike trains. **A:** PSTH displays the rate profile of the used inhomogeneous processes. During period 10 – 12 second, rate had been modulated between 5 and 50 spikes/sec with a Gaussian shape with  $t = 250$  ms, while during Periods 6, 7, 8,  $t = 50$  ms. The rates in Periods 9 and 10 were modulated between 5 and 30 spikes/sec by a step function. **B:** The number of individual and unique JS-patterns of complexities 2 – 6 that were detected in each sliding window ( $\tau_c = 5$ ms, 'SW' = sliding window: 800ms). **C:** The percentage of JS-patterns that show significant difference between two conditions (test-level 5%).

ms, and it performed significance tests on excess or lacking of JSEs between two simulated datasets with complexity 2 to 6. The statistical significance was evaluated for each occurring JS-pattern. We derived the percentage of JS-patterns that occurred significantly different between two conditions. To make comparisons across complexities, the number of significant JS-patterns per complexity was normalized by the total number of identified JS-patterns with corresponding complexity. Between two conditions, spike trains during all the periods were independent, which implied that  $H_0$  should not be rejected, if the actual-false-positive-rate were conservative. The percentage of false rejections of  $H_0$  corresponding to the actual-false-positive-rate is clearly below 5% for all complexities and throughout all sliding windows during all the periods. Therefore, NeuroXidence is a hypothesis test with a conservative actual-false-positive-rate that is affected neither by low rates, rate modulation, latency variability, and cross-trial rate changes, nor by the different model processes (  $\gamma$ -process, Poisson process) used to generate the spike trains.

## 3.4 Method calibration (Part II)

Secondly, we applied NeuroXidence to multivariate cases. As described before, more than two simulated datasets were generated and NeuroXidence was applied to evaluate the JSEs for each simulated data set. ANOVA was applied to the set  $\bar{\Delta}\Theta^k$  to evaluate the significance.

### 3.4.1 False positives for stationary processes

We generated six simulated datasets as six conditions, and each of them has 8 neurons and each spike train is generated by independent and stationary Poisson process. NeuroXidence was then applied to evaluate the false positives of excess or lacking of JSEs among these conditions. Here we also used two

scenarios to generate Poission spike trains for all the conditions.

**Scenario one:** we change the mean spike rates of six simulated datasets together.

**Scenario two:** we set the mean spike rate of one simulated dataset to a fixed value (15 spikes/sec), and changed the mean spike rate of other simulated datasets.

The standard set of parameters for scenario one was defined by 50 trials ( $T_r$ ), mean spike rate of 15 spikes/sec ( $r$ ), 20 surrogates samples ( $S$ ), and  $\eta$  equals 5. From the standard parameter set, 8 different combinations of parameters were derived by varying the number of trials ( $T_r = 20, 50, 100$ ) and the mean spiking rate ( $r_1 = r_2 = 7, 10, 30, 60, 90$  spikes/sec). And the standard set of parameters for scenario two was defined by 50 trials ( $T_r$ ), mean spike rate of 15 spikes/sec ( $r$ ), 1 surrogates samples ( $S$ ), and  $\eta$  equals 5. From the standard parameter set, 8 different combinations of parameters were derived by varying the number of trials ( $T_r = 20, 50, 100$ ) and the mean spiking rate ( $r_1 = 15, r_2 = 7, 10, 30, 60, 90$  spikes/sec). We applied NeuroXidence to each simulated dataset using a sliding window with duration of  $l = 200$  ms. In total, 8 different simulated data models were used to get the false-positive-rate for five JS-patterns of complexity 2 – 6. None of the results from any of the parameter sets shows significant difference among six conditions, for either test-level 5% (Fig. 3.6) or 1% (Fig. 3.7). This shows that NeuroXidence, for multivariate case, can detect additional JSEs among several conditions in a conservative way.

### 3.4.2 Test power for multivariate case

We generated six simulated datasets to stand for six conditions. One of them is modelled as a single-interaction process based on Poisson process, while others were generated by independent homogenous processes. For the single-

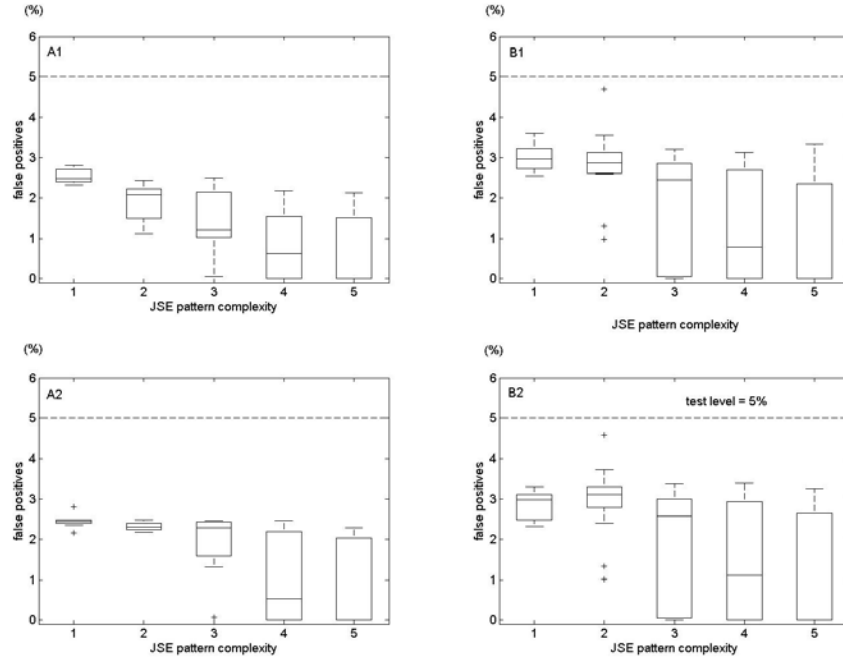


**Figure 3.6: Percentage of false positives estimate by NeuroXidence used to detect joint-spike patterns of complexity 2 to 6 for multivariate cases with test level 5%. Six simulated datasets were generated by independent and homogenous Poisson processes and NeuroXidence was used to estimate JSEs based on 100 independent realizations for each simulated data model. ANOVA was applied to evaluate the false-positive rate of the differences between original data and surrogates data for six conditions. The standard parameter set is as follows: trial= 50, spike-rate= 15 spikes/sec, and  $\eta = 5$ . (A) and (C): mean spike rates of six conditions change together ( $r_1 = r_2 = r_3 = r_4 = r_5 = r_6 = 7, 10, 30, 60, 90$  spikes/sec), after applying NeuroXidence to detect the JS patterns, we applied ANOVA mean test (A) and Kruskal-Wallis test (C) respectively, with variation the number of trials ( $T_r = 20, 50, 100$ ). Here we set surrogate to 20. (B) and (D): we set mean spike rate of condition one to 15, and those of other conditions change from 7 to 90 ( $r_1 = 15, r_2 = r_3 = r_4 = r_5 = r_6 = 7, 10, 30, 60, 90$  spikes/sec), then applied NeuroXidence and ANOVA mean test (B) and Kruskal-Wallis test (D) to evaluate the false positive rates with variation the number of trials ( $T_r = 20, 50, 100$ ). Here we set surrogate to 1.**

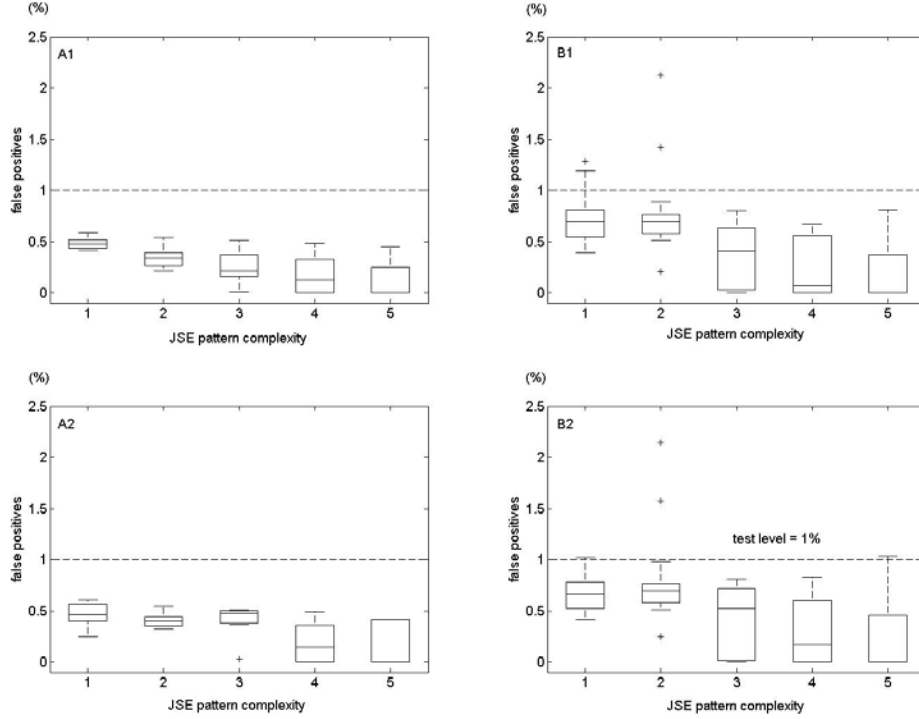


**Figure 3.7: Percentage of false positives estimate by NeuroXidence used to detect joint-spike patterns of complexity 2 to 6 for multivariate cases with test level 1%.** The notation is the same as Fig 3.6.

interaction process, correlated spike trains were characterized by a background rate and a JSE rate. The background rate corresponds to the independent spiking of neurons, while JSE rate defines the expected frequency of the JS-pattern of interest beyond that of other conditions. The standard parameter set is chosen as 50 trials ( $T_r$ ), the background spike rate of 15 spikes/sec ( $r$ ), 20 surrogates numbers ( $S$ ), and  $\eta$  equals 5. Here we show how the test power changes according to different trials ( $T_r = 20, 50, 100$ ) and number of surrogates ( $S = 1, 20$ ). As shown in Fig. 3.8, the test power of higher complexity patterns increases faster than that of lower complexity patterns. Comparing left-hand and right-hand figures, we could find that changing number of surrogates from  $S = 1$  to  $S = 20$  doesn't affect test power so much, which means

NeuroXidence is sensitive enough to detect small difference in JSE frequencies for each JS-pattern. Therefore, in later study number of surrogates can be set to 1, and NeuroXidence still keeps the sensitivity in detecting the JSEs, which are significantly different among several conditions.

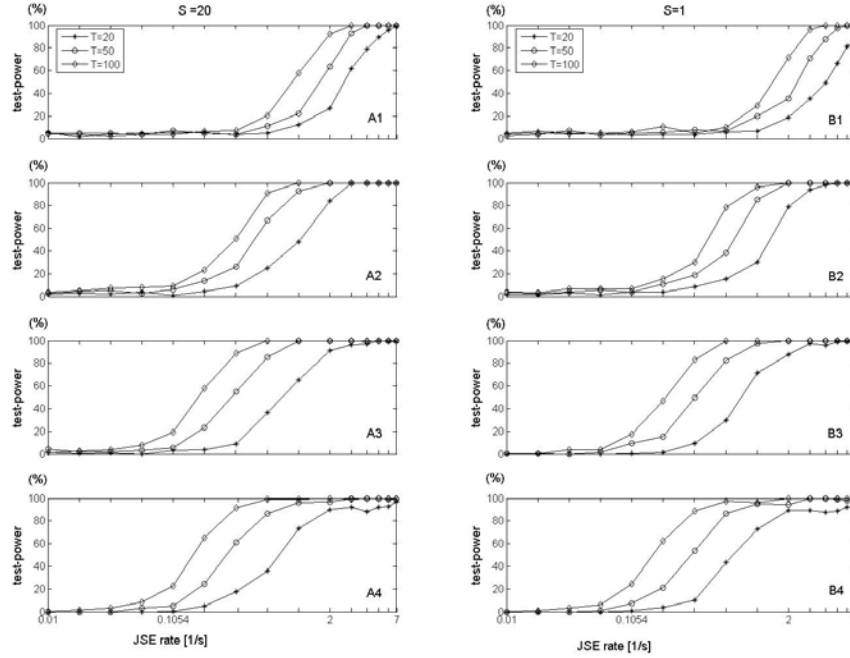


**Figure 3.8: Test power of NeuroXidence in multivariate case.** One simulated dataset was modelled as a single-interaction process based on Poisson process, while the other five simulated datasets were generated by independent and homogenous Poisson processes. NeuroXidence was applied to estimate the JSEs for each simulated dataset. Then ANOVA was applied to evaluate the different frequencies of JSE for each simulated data model. Rows 1 – 4 show the test-power dependencies on the complexities of the analyzed JS pattern ranging from 2 to 5. **(A1-A4)** Test power with surrogates  $S = 20$ . **(B1-B4)** Test power with surrogates  $S = 1$ . The standard parameter set was chosen as  $r = 15$  spikes/sec, and  $\eta = 5$ .

### 3.5 Results of JSEs in short-term-memory experiment

Neuronal activities in short-term memory have been associated with sustained delay firing of prefrontal neurons ([83], [84]). But it is not clear how large populations of neurons store information coordinately. Neuronal interactions in frontal cortex of behaving monkeys have been described to extend over several hundred milliseconds ([85]), while others reported millisecond precise synchrony in prefrontal ([86]) and parietal cortex ([71]). From the calibration results described before, the extension of NeuroXidence showed its reliability and sensitivity of detecting the modulation of occurring frequency of JSEs which are different among several conditions. In this section we applied NeuroXidence on the monkey's short-term memory datasets, investigated the relation of neuronal firing patterns and the process of encoding and maintenance of information during short-term memory. As described in Chapter 2, the dataset contains 2402 trials (7 Sessions / 86 sites) for monkey 1 and 1722 trials (5 Sessions / 66 sites) for monkey 2. In total there are 18150 different JSE patterns for both correct and incorrect responses. In individual experiments, units participate in up to 450 performance-dependent JS-patterns per second. We carried out the analysis in three steps. First we concerned the encoding process of the task and focused on the different modulation of neural synchronized firing between correct and incorrect responses. Then we consider the occurring frequencies of JSEs for the whole task. Thus, we can compare different synchronization of neuronal firing between not only different behavior, but also different processes of the task. Finally, we focused on the stimulus specific modulations of JS-patterns.

As described above, in the first step, we focused on the encoding process of the task and investigated the differences of occurring frequencies of JSEs between



correct and incorrect responses. Raster plots of spikes in the experiment C002 during the sample period are shown in Fig. 3.9. Directly from the raster plot, the spike patterns are quite difficult to identify and there is no obvious difference between correct and incorrect responses of the monkey. After applying NeuroXidence to the datasets, JSEs with different complexities during the sample period are computed. The parameters were chosen as  $\tau_c = 3$  ms and sliding window length  $l = 100$  ms. Then the occurring frequencies of each JS-pattern were compared between correct and incorrect responses. The JS-patterns with significant increases for each condition are shown in Fig. 3.10. From the figure we can see that the occurring time of JS-patterns, especially for higher complexity of JS-patterns, differs a lot between correct and incorrect responses during the sample period. For instance, neurons had stronger synchronization of firing at about 0.3 second after sample onset for correct responses, which is lacking for incorrect responses.

To illustrate the rate changes for the encoding process, we derived the PSTH (bin-width: 5 ms) based on 27 single-unit activities during the sample period in experiment C002 (Fig. 3. 11 (A1) and (A2)). It turns out that the rate increased from about 125 ms after sample onset. However, there is no difference between (A1) and (A2), which is corresponding to the PSTH of correct and incorrect responses respectively. NeuroXidence was then applied to the same datasets and the occurring frequencies of JSEs were computed. The timescale for synchronized firing was chosen as 3 ms. Based on the occurring frequencies of JS-patterns, we computed how often each individual neuron participated in JS-patterns that showed performance-related modulation of synchrony. To be more specific, we compared the occurring frequencies of JS-patterns between correct and incorrect responses, and concentrated on the JS-patterns which shows significant increase for each condition. Thus, after calculating the frequencies that each neuron participated in these JS-patterns, the re-

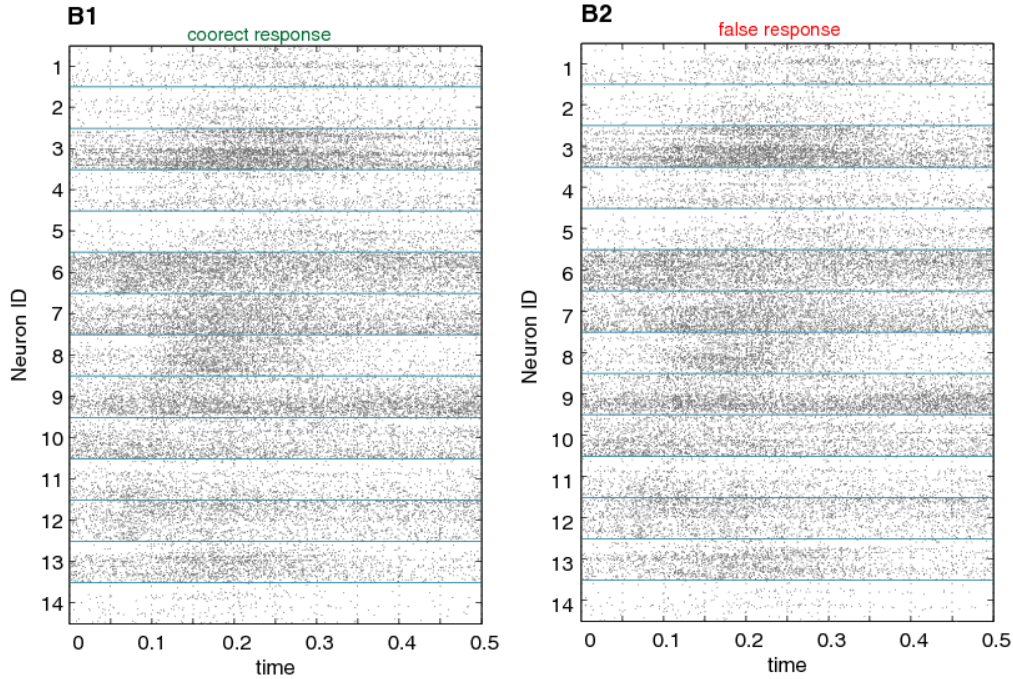


**Figure 3.9: Raster plot of spikes for different responses of monkey.** Raster plot of 14 out of 27 cells simultaneously recorded in a single dataset C002. **(B1)** shows the spikes for correct response of the monkey, while **(B2)** shows those for incorrect response.

sults for each condition are shown in Fig. 3.11 (B1) and (B2). Each neuron could participate in more than one JS-pattern, and there are some neurons that participated in up to 400 performance-modulated JS-patterns. After the sample onset, the different modulation of synchronized firing occurred mainly after 125 ms. More neurons fired synchronously for correct than for incorrect responses. However, before 125 ms, there are still some neurons firing synchronously for correct responses. The difference between correct and incorrect results was shown in (B3). This figures tells us that more neurons had coordinate firing for correct responses than for incorrect responses during the sample period. Thus, the coordinate firing of neurons might be the key point for the monkey to encode the sample properly.

In the second step, NeuroXidence was applied to the whole period of the task

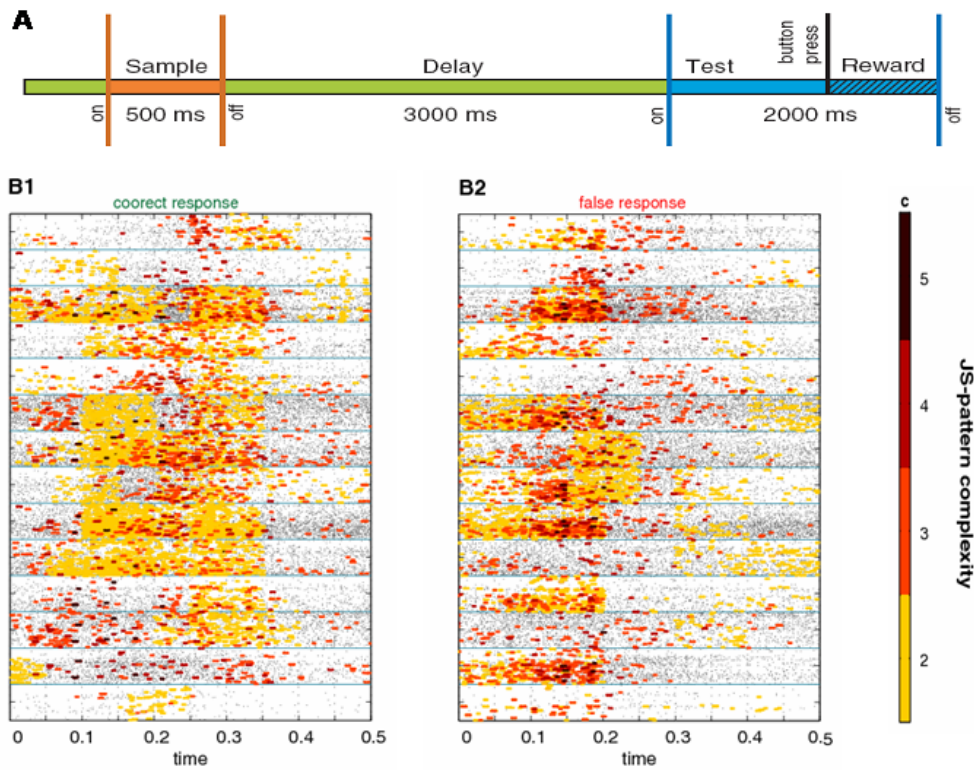


**Figure 3.10: JS-patterns for different responses of monkey.** (A) Time course of the visual short-term memory task. (B1, B2) Raster plot of 14 out of 27 cells simultaneously recorded in a single dataset C002. Joint-spike activity patterns are indicated with squares. All the JS-patterns shown in (B1) indicate neurons had stronger synchronized firing for correct responses than for incorrect responses, while in (B2) shows the opposite. Each square marks the spike that participated in the JS-pattern, which showed performance-modulated synchronized firing in a window of 3 ms. Different colors indicate different JS-pattern complexities. Yellow indicates synchronous activity of pairs of neurons (duplets), while dark red symbolizes synchronous activities of at least 5 neurons (quintets) in 3 ms time frame.

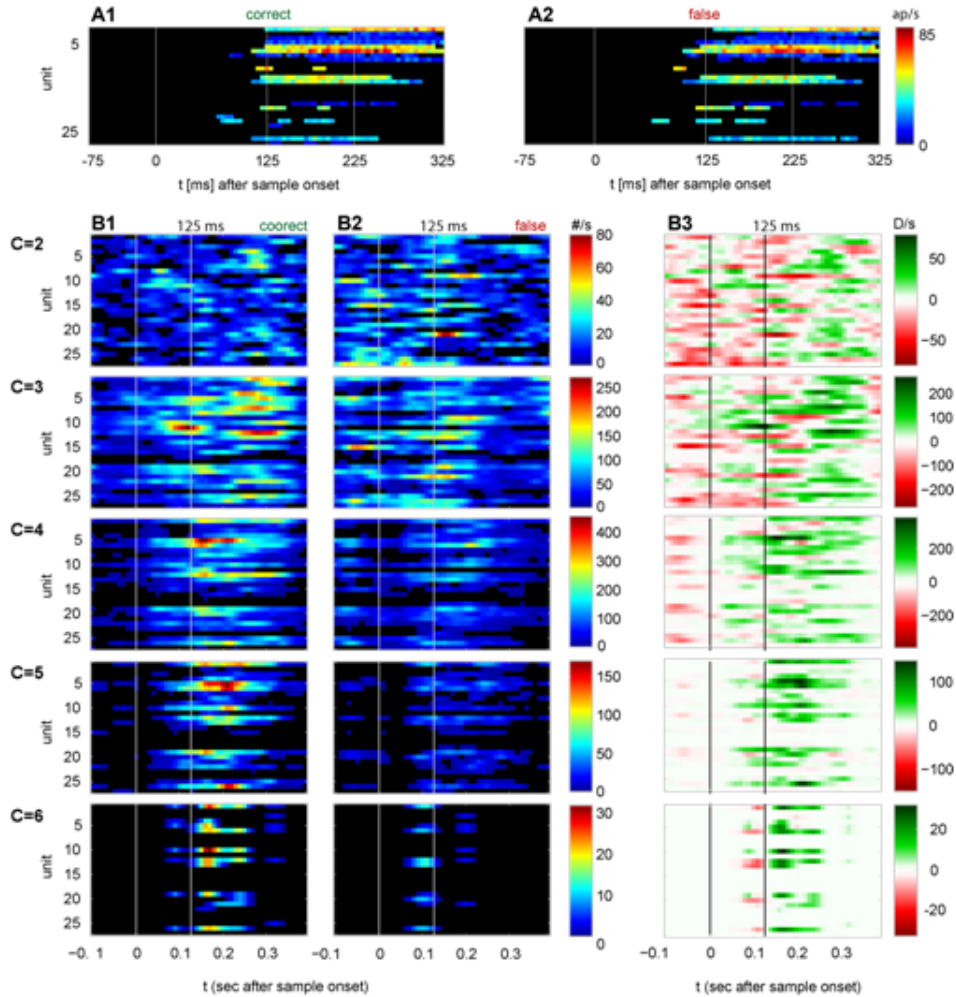


**Figure 3.11: PSTH and JSEs for different responses of monkey.** For the same data as shown in Fig. 3.10, but for all 27 single-unit-activity that were recorded simultaneously. We derived the PSTH (bin-width= 5 ms) for all correct (**A1**) and incorrect trials (**A2**). (**B1**) shows how often a neuron participates in the JS-patterns, on a timescale  $\tau_c$  of 3 ms, that are more synchronous for correct trials, while (**B2**) shows the opposite. (**B3**) shows the difference between (B1) and (B2). Green indicates that a neuron participates more often in JS-patterns that are more synchronous for correct trials.

and compared the occurring frequencies of JSEs between monkey's different behavior. The parameters of NeuroXidence were chosen as 1 surrogate numbers ( $S$ ), 3 ms of precise timing of JSE ( $\tau_c$ ), and scale separation equals 3 ( $\eta$ ). Due to the non-stationary properties of the process, we applied NeuroXidence with the sliding window (window length: 400 ms) analysis. The results are shown in Fig. 3.12. Comparing (A1) and (B1), we can see that, for different responses of the monkey, synchronization of neuronal firing occurred at different time points. To be more specific, the most prominent synchronization of neuronal firing was observed in complexity 3 to 7 JS-patterns during sample and early delay in correct trials, which yielded the occurring frequencies of JSEs above 30. In contrast, the maximal occurring frequencies of JSEs during these periods in incorrect trials only reached values that were about 15. This difference between correct and incorrect responses is much clearer when we examined the results during the sample period (Fig. 3.12 (A2),(B2)). Thus, in correct trials, more neurons fired synchronously during the sample and early delay period, which is corresponding to the encoding and maintenance process respectively.

Then, we shuffled the correct and incorrect trial sets and recomputed the difference between permuted 'correct' and 'incorrect' results. In this step, since we only shuffled the correct and incorrect trial sets and kept other properties of the data, we can tell whether the original difference of frequencies of JSEs is coming from the different responses of the monkey. From the results of the permuted classes (Fig. 3.13 (B)), we can see that the dominate color of the figure is white, which means there is almost nothing different between permuted 'correct' and 'incorrect' trial sets. Based on the original and permuted difference, we computed the z-score of the original difference of correct and incorrect responses. For each complexity and sliding window, the z-score is computed given the absolute difference between correct and incorrect results,

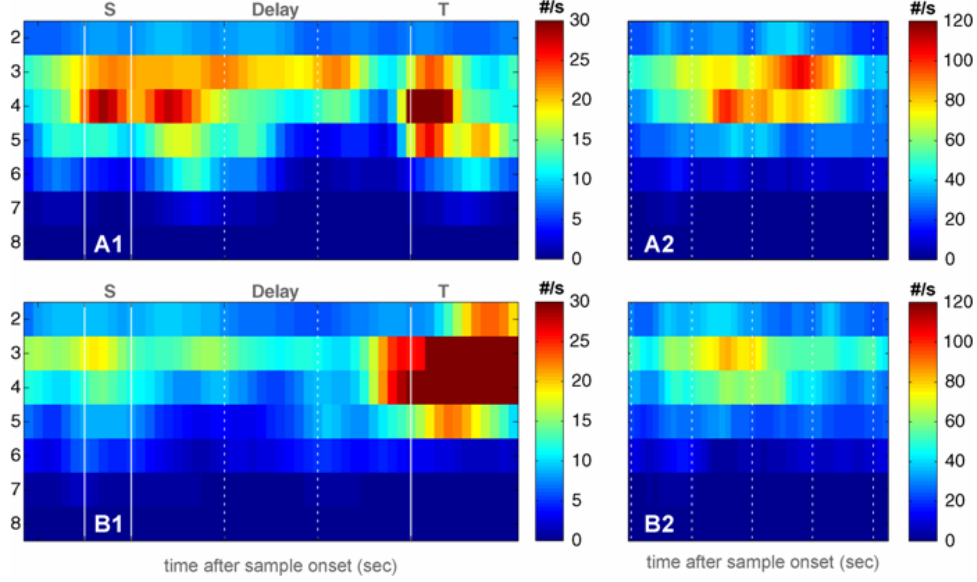


**Figure 3.12: JSEs for different responses of monkey.** (A) Frequency of occurrence of JS-patterns of complexities 2 to 8 with performance correlated increases of synchrony in correct trials. On the contrary, figure (B) shows the frequency of occurrence of JS-patterns with performance correlated increases of synchrony in incorrect trials. The left column (A1), (B1) shows the analysis for 400 ms long sliding windows and the whole temporal cores of the paradigm, including 600 ms of baseline activity. In addition, (A2), (B2) shows the same but with 100 ms long sliding windows and only for the period during sample presentation.

and divided by the standard deviation of the difference for permuted 'correct' and 'incorrect' trial sets. To be more specific, similar with Equation (2.3.2), we defined z-score here as

$$z \equiv \frac{\lambda - E\{\lambda_p\}}{\sigma_{\lambda_p}} \quad (3.5.1)$$

. where  $\lambda$  is the difference of frequencies of JSEs, and  $\lambda_p$  stands for the  $\lambda$  value of the permuted results. From Fig. 3.13 (C), we can see that when the monkey had the correct response, there is a significant excess of JSE

with complexity 3 to 7 JS-pattern during the sample and early delay, which means performance-related modulation of synchrony occurred mainly during the process of information encoding and maintenance. Thus, the task- and performance-dependent modulation of synchrony reflects that the dynamic formation of group of neurons contributes to short-term memory.

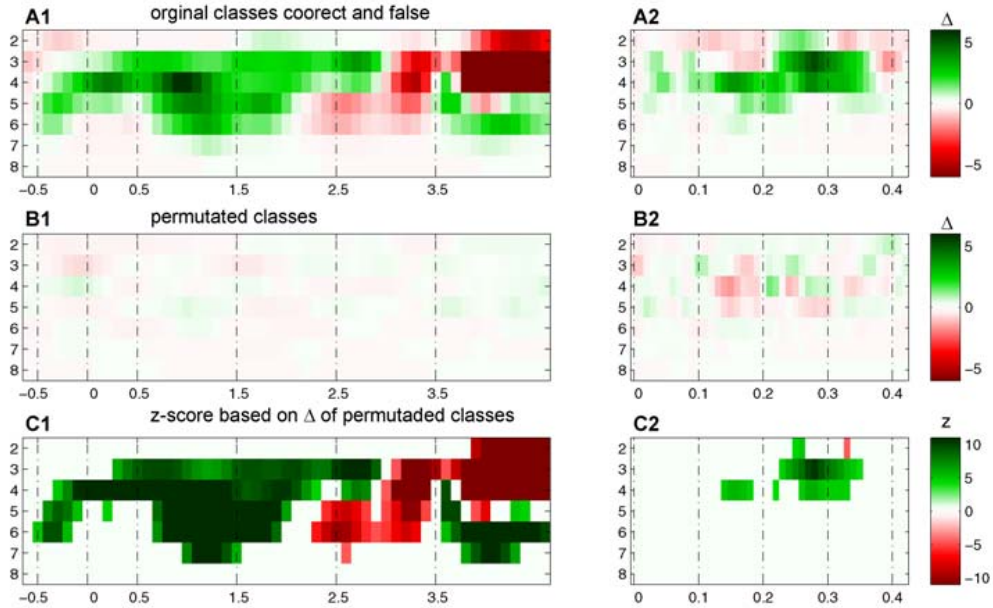


**Figure 3.13: Significance results of JSEs for different responses of monkey.** Fig. (A) shows the difference between the frequencies of JS-patterns with increases of synchrony for correct and incorrect behavior. (B) shows the difference between permuted 'correct' and 'incorrect' trial sets. Based on the average level of differences in (B) and the standard deviation of these differences, the difference in (A) was expressed as a z-score in (C). The critical z-value is 4.2 given a test-level of 1% and a Bonferroni correction for 48 sliding windows and 7 complexities.

In the final step, we evaluated the modulation of stimulus specific JS-patterns.

For monkey's correct responses, we used the identical datasets and the identical number of trials per stimulus, but permuted the stimulus randomly across all trials and recomputed the frequencies of JS-patterns. Then, the z-score is derived based on the difference between the numbers of JS-pattern with stimulus specific modulation of synchrony for the original stimulus classes and the permuted stimulus classes. Thus, statistical evaluation of the frequency is shown in Fig. 3.14 (A). In a second step, this difference is normalized by the standard deviation of the frequency for permuted classes (Fig. 3.14 (B)). This normalization is done for each individual complexity and based on the standard deviation evaluated across the whole time course starting at  $-0.5$  s and ending at 4.3 s. It turned out that the JS-patterns with complexity 3 to 5 had a strong modulation with some specific stimulus, especially during the test period.

## 3.6 Spike-spike coherence and joint-spike-event

Since coherence reveals the basic linear pair-wise relations between two signals, it can also be applied to two point processes - spike signals. Meanwhile, NeuroXidence is a proper tool to detect the co-activities of groups of neurons. Thus, we compared the results based on these two methods and investigated whether the pair-wise relation is good enough to detect the performance-dependent changes of the short-term memory task. We applied multitaper method as described in Chapter 2 to compute the spike-spike coherence. The standard parameters were chosen as window length 200 ms, window shift 20 ms, 4 DPSS tapers with order 0 to 3. The grand average of the experimental results are shown in Fig. 3.10. Since the spike spectrum has a broad dynamic range, when spike-spike coherence was computed by means of cross-spectra in frequency domain, the difference between the results of correct and incorrect responses are subtle and hardly to detect.



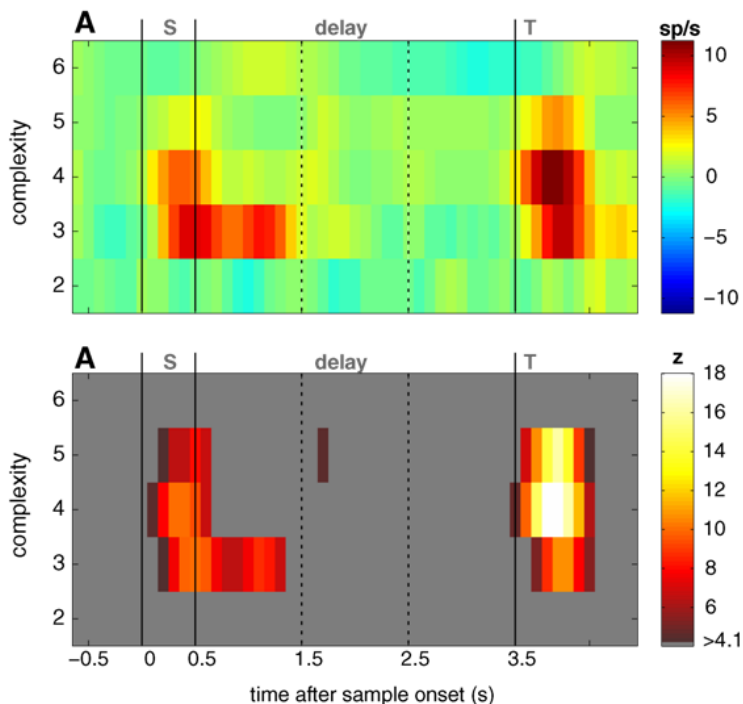


**Figure 3.14: Stimulus specific JS-patterns.** (A) Frequency of occurrence of JS-pattern of complexities 2 to 6 with stimulus specific modulation. (B) shows the z-score of (A). The critical z-value was 4.08 given a test-level of 1% and a Bonferroni correction for 48 sliding windows and 5 complexities.

Permutation test was then applied to detect the significant modulations due to behavioral performance. The results are shown in Fig. 3.11. Comparing the spike-spike coherence of correct and incorrect responses, we can see the different modulations due to monkey's different responses occurred during pre-sample, sample, early delay, late delay and test period. When the monkey had a correct response, there is a significant increase of spike-spike coherence of  $\gamma$ -band during these periods. This result is in the line with the results of NeuroXidence. Since the NeuroXidence reveals more than pair-wise relation between neurons, it can provide a better explanation of the synchronous firing of the neurons. As we mentioned the sub- and supra-patterns before, the

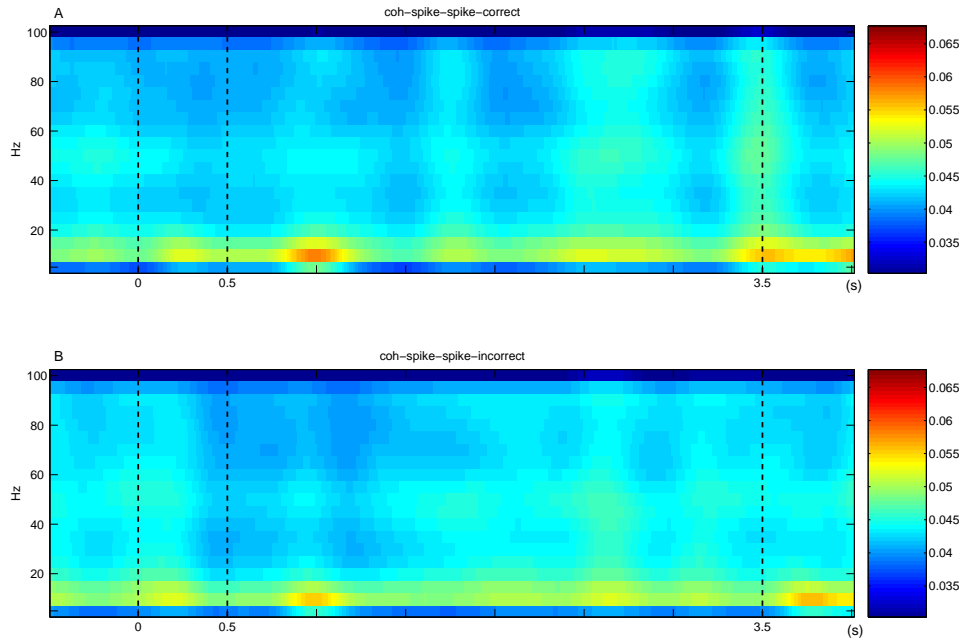


**Figure 3.15: Grand average time-frequency ('TF') plots of spike-spike coherence. (A)** The grand average of spike-spike coherence for trials with correct response. **(B)** The grand average of spike-spike coherence for trials with incorrect response.

existence of supra-pattern JSE could lead to an increase of JSE in the sub-patterns. Thus, during the short-term memory task, neurons in monkey's prefrontal cortex might fire synchronously, especially in groups of 3 – 7, to ensure the correct response.

### 3.7 Discussion

It has been shown before the detection of JSEs by NeuroXidence is reliable and robust for univariate case ([78, 79]). The method is therefore optimized to detect synchronous firing beyond that expected by chance reliably, but does not allow to compare the strength across factors, or suitable for comparing differ-

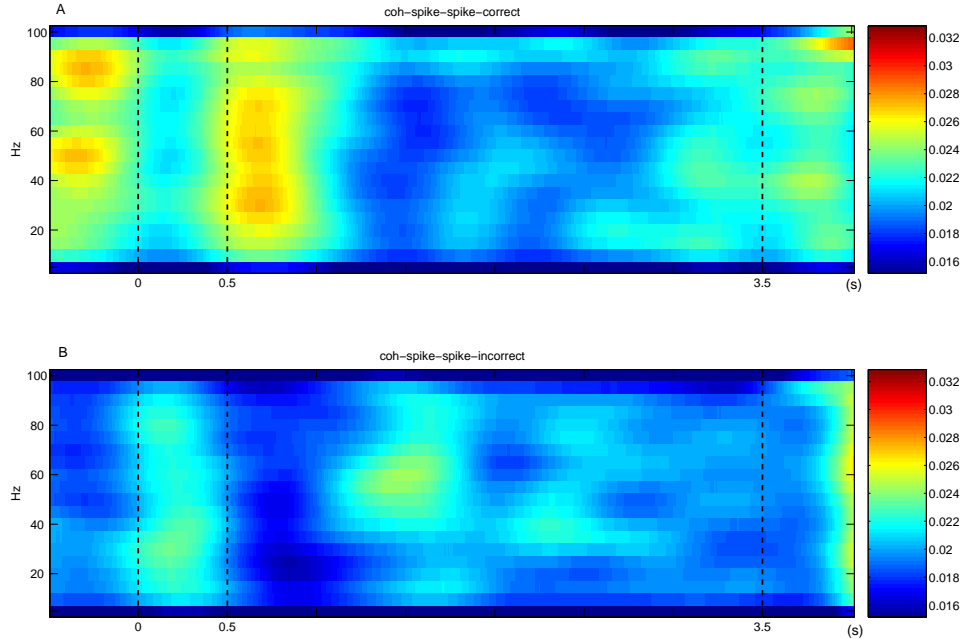


**Figure 3.16: Performance-dependent increase of  $\gamma$ -oscillations in spike-spike coherence in prefrontal area. (A)** Time-frequency  $\lambda_c$ -maps. It provides the percentage of sites/pairs with significant increases of spike-field coherence in trials with correct responses. **(B)**  $\lambda_f$ -maps shown provides the results of incorrect response.

ent factors and was not robust against features that were discussed to induce false positives. After extending the method to bi- and multi-variate cases, NeuroXidence method keeps its advantage of detecting the different modulation of JSEs among different factors. Especially in the non-stationary process, NeuroXidence rejects the artifact, which different processes ( $\gamma$ -process, Poisson process and latency covariations) bring to the occurring frequencies of JSEs. As for the test power, on average only 2 JSEs more or less than other conditions can be detected, which exhibits the high sensitivity of NeuroXidence for the bi- and multi-variate cases. When NeuroXidence was applied to

detect JSEs in the processes with different rate level, except for  $\tau_c$  and  $\tau_r$ , surrogates number ( $S$ ) becomes another important parameter in the method. To be more specific, when NeuroXidence is applied to two or more processes with different rates, especially some of the processes with low firing rates, number of surrogates should be set to 1 to ensure the non-biased estimates of JSEs. After applying NeuroXidence to the monkey's short-term memory data, it reveals that neurons in prefrontal cortex fired synchronously during the early delay and sample period for monkeys to make the correct response. This result is consistent with that of spike-spike coherence analysis. Furthermore, comparing the results from NeuroXidence and spike-spike coherence, NeuroXidence showed its unique way of detecting the high-order relations among groups of neurons, which is lacking in the spike-spike coherence analysis.

### 3.8 Summary

Extended to bi- and multi-variate cases, NeuroXidence remains its sensitive and conservative properties of detecting coordinate firing events for different factors. Based on this extension, we found in monkey's prefrontal cortex during short-term memory task, encoding and maintenance of the information rely on the formation of neuronal assemblies characterized by precise and reliable synchronization of spiking activity on a millisecond time scale.

# Chapter 4

## Discussion

### 4.1 Multitaper method, permutation test and NeuroXidence

When we analyzed the datasets from monkey prefrontal cortex during short-term memory task, three main methods were applied: multitaper method, permutation test and NeuroXidence method. The first two were applied to evaluate the spike-field coherence, while the last one was used to detect different JS patterns.

#### 4.1.1 Multitaper method

Spectral analysis is carried out in frequency domain, which could reveal the information of the underlying oscillation of the process. It has several advantages comparing with time domain methods. Especially for the spike signal, which people deal with as point process, spectral analysis smoothes the spike signal in a proper way and treats it as a continuous one. Thus the rhythm of the spikes and the relations between spikes and other continuous signals can be studied.

Multitaper method is a special spectral analysis that people apply to reduce the leakage and concentrate power. The direct spectral estimator is severely biased when the process has a large dynamic range. Multitaper method overcomes this problem by averaging the spectral estimates from several orthogonal tapers. Furthermore, after applying multitaper method, the bias and confidence interval of the analysis can be estimated in a simple way. We applied multitaper method to the monkey's short-term memory datasets and it revealed that when the datasets are large enough, the extra smoothing of multitaper method is not necessary to decrease the variance or make the important frequency component more obvious. From Fig. 2.4 we can see that sometimes multitaper method could even obscure the important frequency component by the additional smoothing.

#### **4.1.2 Permutation test**

Permutation test is a non-parametric statistical tool. It provides a simple and proper way to derive the  $H_0$  hypothesis with no additional mathematical assumptions. After applying permutation test, based on the spectral results of spike-field coherence, we got the  $\lambda$  value for monkey's different responses. Comparing the results of the experimental and simulated datasets, we found that the  $\lambda$  values of experimental and simulated datasets are in the same range. After corrected for the baseline effect, the values are still compatible. This shows permutation test is a robust and powerful tool to evaluate the significance of the results.

#### **4.1.3 NeuroXidence method**

In the last years, there are two different ways for people to interpret neuronal coding: single cell coding or cooperative neuronal coding. One is based on spike rate and the other is base on the assembly spike patterns. NeuroXidence

method is a newly developed method that belongs to the second type. It has already been shown that the detection of JSEs by NeuroXidence is reliable, sensible and robust for uni-variate case. The two important parameters  $\tau_c$  and  $\tau_r$  determines the precise spike patterns and the spike rate modulation range, respectively. After extending to bi- and multi-variate case, NeuroXidence method remains its advantage of detecting the modulation of JSEs which are different among several conditions, especially NeuroXidence methods separates the rate and assembly patterns coding in the non-stationary processes (Fig. 3.5). No matter how the process changes, from  $\gamma$ -process to Poission process or even latency covariations, the JSEs that NeuroXidence detected among several conditions is still below the chance level. When several different processes were analyzed by NeuroXidence, only 2 JSEs more/less among different processes can be detected, which exhibits the high sensitivity of NeuroXidence for the bi- and multi-variate cases. If NeuroXidence is applied to detect JSEs in processes with different rate level, except for  $\tau_c$  and  $\tau_r$ , surrogates number ( $S$ ) becomes the most important parameter in the method. Number of surrogates should be set to 1 to ensure the non-biased estimates of JSE of different rate level processes.

## 4.2 Short-term memory process in monkey prefrontal cortex

Based on the three methods mentioned above, we analyzed the spike and local field potential signals from prefrontal cortex of two monkeys who performed a visual discrimination task. Since the monkey had correct and incorrect responses, we compared the results from each response and tried to find the difference between different behavioral performance.

After applying multitaper method and permutation test, we found the modu-

lation of two frequency bands (5 – 20 Hz, 25 – 70 Hz) are completely different. Since the results come from a rather small percentage of significant pairs of spike-field coherence, we generated the simulated datasets and applied the same methods to the simulated datasets. It turned out that the results of simulated and experimental datasets are compatible. This demonstrates that even though the variability of individual spike-field coherence estimates might be rather large, assessments of performance-related differences of  $\lambda$  based on a large number of estimates is highly reliable. Quantitative comparison of the two types of simulated data, the one modeling phase-precision and the one modeling the strength of synchronization, illustrates that experimental results in the high-frequency band are most likely based on precisely phase-locked spikes that have a low probability of occurrence. Given the results of the simulated data analysis, spikes must be locked with a precision of less than 2 ms to local field potential oscillations at 50 Hz (phase-precision:  $0.2\pi$ ) to reach  $\lambda$  values close to the maximal values (3.5%) observed in the experimental results. However, given the rather short period ( $w = 2$  ms), an oscillation frequency of 50 Hz, and a rate  $r_1 = 25$  spikes/sec, we expect 0.5 phase-locked spikes per sliding window. This illustrates, first, that the method is very sensitive and second, that differences in spike-field coherence due to behavioral performance might be based on rather few synchronous events in prefrontal cortex, which cannot be explained by chance.

After applying the extension of NeuroXidence to the monkey’s short-term memory datasets, the occurring frequencies of JS-patterns show different modulations for correct and incorrect responses of the monkey. The differences of frequencies of JSEs between behavioral performance are in the range of  $-5$  to  $5$ . The strongest increase of synchrony in correct trials occurs during early delay. Performance related modulation of synchrony exists in JS-pattern complexities from 3 to 7. The complexity 2 JS-pattern, which corresponds to the



pair-wise JS-pattern, are not performance modulated. When we permuted the trial-sets between correct and incorrect responses, the difference of JS-patterns for permuted behavioral performance is no longer significant. This shows that assembly of neurons in prefrontal cortex fired synchronously during the early delay and sample period for monkeys to make correct response. This result is consistent with that of spike-spike coherence analysis.

# Chapter 5

## Conclusion

### 5.1 Scale Integration

Based on the results of spike-field coherence, the underlying process of short-term memory seems to involve networks of different sizes within and, most probably, beyond prefrontal cortex. Spikes, which were generated by single neurons, cooperate with local field potentials, which were the slower fluctuations of the environment. Although differences among behavioral conditions appear to be based on rather few instances of phase-locked spikes, the task-related effects on spike-field coherence are highly reliable and cannot be explained by chance, as the comparison of results from experimental and simulated data shows. The differential locking of prefrontal neuron populations with two different frequency bands in their input signals suggests that neuronal activity underlying short-term memory in prefrontal cortex transiently engages cortical circuits on different spatial scales, probably in order to coordinate distributed processes.

## 5.2 NeuroXidence method and Synchronized firing

Based on the results of the calibration datasets, for bi- and multi-variate cases, the extension of NeuroXidence remains its sensitivity and reliability of detecting coordinate firing events for different processes. Based on this extension of NeuroXidence, we demonstrated that in monkey's prefrontal cortex during short-term memory task, encoding and maintenance of the information rely on the formation of neuronal assemblies characterized by precise and reliable synchronization of spiking activity on a millisecond time scale, which is consistent with the results from spike-spike coherence. The task and performance dependent modulation of synchrony reflects the dynamic formation of group of neurons has large effect on short-term-memory.

# Appendix A

## Appendix: Coherence

The coherence function is a measure based on the spectral properties of the processes. The coherence function, or squared coherence, is defined as

$$coh_{xy}^2(f) = \frac{|S_f(xy)|^2}{|S_f(x)|^2|S_f(y)|^2} \quad (1.0.1)$$

Since the absolute value of  $|S_f(xy)|^2$  has the range from 0 to  $|S_f(x)|^2|S_f(y)|^2$ ,  $coh_{xy}^2(f)$  could be interpreted as the square of the cross spectrum normalized by the product of the auto-spectra. The normalization is very important because it guarantees that only the coupling between two processes is considered. For example, if  $X$  or  $Y$  process has larger power at some frequency  $f$  and leads to the large values of the cross spectrum, the normalization compensates this phenomenon. If the  $X$  and  $Y$  processes are identical, it is valid that at all frequencies  $|S_f(xy)| = |S_f(x)|^2 = |S_f(y)|^2$  and  $coh_{xy}^2(f) = 1$ . On the contrary, if  $X$  and  $Y$  are totally independent, it follows that at all frequencies  $S_f(xy) = 0$  and  $coh_{xy}^2(f) = 0$ . Between these two extremes, coherence function reveals different possible relations between the processes. For example, if  $X$  and  $Y$  are strongly coupled only over a limited range of frequencies, which could be the case if  $X$  and  $Y$  both have strong responses to a sinusoidal signal of frequency  $f_0$ , the coherence function is nearly 1 at  $f_0$  and zero elsewhere. Meanwhile, the coherence function suppresses any phase information of the

single process, since it considers the relationship between two processes only in terms of power at a given frequency.

Coherence is a useful frequency-domain function, which makes a rough description of the relations between two processes. However, the estimator  $coh_{xy}^2(f)$  in the coherence function should be defined carefully. Since the coherence function estimator based on raw auto- and cross-spectra cannot have a meaningful interpretation, it requires the spectra to be smoothed before computing the coherence. Thus it requires more concern to the smoothing process of auto- and cross-spectra, especially the bias and resolution during the smoothing. Their effect on the coherence function estimator is more difficult to determine, simply because of the way that coherence function is defined. Although the general solutions for the bias and resolution of coherence function estimator haven't been achieved, the main interesting property of coherence is that the estimator from the smoothed spectral estimates is quite robust. That is to say, this estimator is not sensitive to the Gaussian or non-Gaussian processes. Thus one can apply coherence function estimator with no concern on whether the results of the analysis are sensitive to the amplitude distributions of the particular process.

# Appendix B

## Appendix: Bonferroni correction

In statistics, Bonferroni correction is one of the multiple-comparison correction methods. It requires that, if  $n$  independent hypotheses are tested on a set of data, the statistical significance level for each hypothesis should be  $1/n$  times as it would be if only one hypothesis is tested. For instance, if two independent hypotheses are tested on the same data with significance level 0.05, one should use the  $p$ -value threshold of  $1/2 * 0.05 = 0.025$  for each of the hypothesis.

The Bonferroni correction guarantees the validity of the hypothesis test on multiple-comparison conditions. Without the multiple-comparison corrections, 1 out of 20 independent hypothesis-tests will appear to be significant with significance level 0.05, which is purely due to chance.

# List of Figures

1.1	An action potential recorded intracellularly from a cultured rat neocortical pyramidal cell. . . . .	4
1.2	Extracellular recording in the tissue. . . . .	5
1.3	The four lobes of the cerebral cortex. . . . .	12
1.4	Schematic description of short-term-memory tasks used to test the function of prefrontal cortex. . . . .	15
1.5	Subdivisions of the macaque prefrontal cortex . . . . .	16
2.1	Time course of visual short-term memory task. . . . .	19
2.2	MRI-based reconstruction of recording positions. . . . .	21
2.3	Basic principles of the permutation test. . . . .	24
2.4	Grand average time-frequency ('TF') plots for spike-field coherence. . . . .	26
2.5	$\lambda$ -map of Session 5122 with different permutation replications	27
2.6	Performance-dependent increase of $\gamma$ -oscillations in spike-field coherence in prefrontal area. . . . .	28
2.7	Time course of significance for spike-field coherence with respect to the pre-sample period. . . . .	30
2.8	Test power of simulated data. . . . .	33

3.1	Percentage of false positives estimate by NeuroXidence used to detect joint-spike patterns of complexity 2 to 6 for bivariate cases with test level 5%. . . . .	40
3.2	Percentage of false positives estimate by NeuroXidence used to detect joint-spike patterns of complexity 2 to 6 for bivariate cases with test level 1%. . . . .	41
3.3	Test power of NeuroXidence in relation to the number of trials ( $T_r$ ), spike rate( $r$ ) and number of surrogates ( $S$ ) in bi-variate case. . . . .	43
3.4	Test-power of NeuroXidence for an induced mother-pattern and its supra-patterns and sub-patterns. . . . .	45
3.5	False positives for a non-stationary process evaluated by NeuroXidence. . . . .	46
3.6	Percentage of false positives estimate by NeuroXidence used to detect joint-spike patterns of complexity 2 to 6 for multivariate cases with test level 5%. . . . .	49
3.7	Percentage of false positives estimate by NeuroXidence used to detect joint-spike patterns of complexity 2 to 6 for multivariate cases with test level 1%. . . . .	50
3.8	Test power of NeuroXidence in multivariate case. . . . .	51
3.9	Raster plot of spikes for different responses of monkey. . . . .	54
3.10	JS-patterns for different responses of monkey. . . . .	55
3.11	PSTH and JSEs for different responses of monkey. . . . .	56
3.12	JSEs for different responses of monkey. . . . .	58
3.13	Significance results of JSEs for different responses of monkey. . . . .	59
3.14	Stimulus specific JS-patterns. . . . .	61
3.15	Grand average time-frequency ('TF') plots of spike-spike coherence. . . . .	62



3.16 Performance-dependent increase of  $\gamma$ -oscillations in spike-spike coherence in prefrontal area. . . . . 63

# List of Variables

$\Theta$	test statistic
$H_0$	null hypothesis
$\sigma$	variance
$E$	expectation
$B$	number of bootstrap sample
$T_r$	number of trials
$S$	number of surrogates
$f$	frequency of a JSE
$f_{org}$	frequency of a JSE in the ordinal data
$f_{sur}$	frequency of a JSE in the surrogate data
$\eta$	scaling factor between $\tau_c$ and $\tau_r$
$\tau_c$	temporal time scale of JSE
$\tau_r$	temporal time scale of of cross-structure considered a rate
$\lambda_c$	percentage of tf-bins with increased spike-field coherence for correct
$l$	length of analysis window in units of seconds
$z$	z-value = mean/std
$\nu_0$	degree of freedom
$K_t$	number of tapers
$N_0$	natural number
$Q$	real number
$k$	Index of JS-pattern with $k = 1 \dots K$
$K$	Number of distinct JS-pattern for each sliding window
$\Delta f_{t,\xi}^k$	difference between $f_{org}$ and $f_{sur}$ for trial t, condition $\xi$ and JS-pattern k
$\bar{\Delta} f_{t,\xi}^k$	mean difference between $f_{org}$ and $S$ estimates of $f_{sur}$
$\bar{\Delta} F_{\xi}^k$	set of $\bar{\Delta} f_t^k$ for $T_r$ trials
$coh_{xy}$	coherence of processes X and Y
$S_f(x)$	spectrum of process X

## Bibliography

- [1] Adrian ED (1928) *The basis of sensation: The action the sense organ*. Christophers, London.
- [2] Hodgkin AL, Huxley AF (1939) Action potentials recorded from inside a nerve fibre. *Nature* 144: 710-711.
- [3] Dayan P, Abott LF (2001) *Theoretical Neuroscience: Computational and Mathematical Modeling of Neural Systems*. The MIT Press, Cambridge.
- [4] Lewicki MS (1998) A review of methods for spike sorting: the detection and classification of neural action potentials. *Network Comput. Neural Syst.* 9: R53-R78.
- [5] Harris KD, Henze DA, Csicsvari J, Hirase H, Buzsaki G (2000) Accuracy of tetrode spike separation as determined by simultaneous intracellular and extracellular measurements. *J. Neurophysiol.* 84: 401-414.
- [6] Fee MS, Mitra PP, Kleinfeld D (1996) Automatic sorting of multiple unit neuronal signals in the presence of anisotropic and non-Gaussian variability. *J. Neurosci. Methods* 69: 175-188.
- [7] Legatt AD, Arezzo J, Vaughan HG (1980) Averaged multiple unit activity as an estimate of phasic changes in local neuronal activity: effects of volume-conducted potentials. *J. Neurosci. Methods* 2: 203-217.

- [8] Singer W, Gray CM (1995) Visual feature integration and the temporal correlation hypothesis. *Annu. Rev. Neurosci.* 18: 555-586.
- [9] Juergens E, Guettler A, Eckhorn R (1999) Visual stimulation elicits locked and induced gamma oscillations in monkey intracortical- and EEG-potentials, but not in human EEG. *Exp. Brain Res.* 129: 247-259.
- [10] Glaser EM, Ruchkin DS (1976) *Principles of Neurobiological Signal Analysis*. Academic Press Inc., Orlando.
- [11] Wilson MA, McNaughton BL(1993) Dynamics of the hippocampal ensemble code for space. *Science* 261: 1055-1058.
- [12] Brillinger DR (1992) Nerve cell spike train data analysis: a progression of techniques. *J. Amer. Stat. Assoc.* 87: 260-271.
- [13] Brillinger DR (1978) Comparative aspects of the study of ordinary time series and of point processes. in *Developments in Statistics* Vol. 1: 33-129 (Academic Press, Orlando).
- [14] Jarvis MR, Mitra PP (2001) Sampling properties of the spectrum and coherency in sequences of action potentials. *Neural Comput.* 13: 717-749.
- [15] Percival DB, Walden AT (2000) *Wavelet Methods for Time Series Analysis*. Cambridge Univ. Press, Cambridge.
- [16] Abeles M (1982) Quantification, smoothing, and confidence limits for single-unit histograms. *J. Neurosci. Methods* 5: 317-325.
- [17] Softky WR, Koch C (1993) The highly irregular firing of cortical cells is inconsistent with temporal integration of random EPSPs. *J. Neurosci.* 13: 334-350.

- [18] Shadlen MT, Newsome WN (1998) The variable discharge of cortical neurons: implications for connectivity, computation, and information coding. *J. Neurosci.* 18: 3870-3896.
- [19] Martignon L, *et al.* (2000) Neural coding: high-order temporal patterns in the neurostatistics of cell assemblies. *Neural Comput.* 12: 2621-2653.
- [20] Abeles M, Gerstein GL (1988) Detecting spatiotemporal firing patterns among simultaneously recorded single neurons. *J. Neurophysiol.* 60: 909-924.
- [21] Grün S, Diesmann M, Aertsen A. (2002) Unitary events in multiple single-neuron spiking activity: II. Nonstationary data. *Neural Comput.* 14: 81-119.
- [22] Gütig R, Aertsen A, Rotter S. (2002) Statistical significance of coincident spikes: count-based versus rate-based statistics. *Neural Comput.* 14: 121-153.
- [23] Pipa G, Grün S. (2003) Non-parametric significance estimation of joint-spike events by shuffling and resampling. *Neurocomputing* 52-54: 31-37.
- [24] Pawitan Y (2001) *In All Likelihood: Statistical Modelling and Inference Using Likelihood..* Oxford Univ. Press, New York.
- [25] Brillinger DR (1988) Maximum likelihood analysis of spike trains of interacting nerve cells. *Biol. Cybern.* 59: 189-200.
- [26] Barbieri R, Quirk MC, Frank LM, Wilson MA, Brown EN (2001) Construction and analysis of non-Poisson stimulus response models of neural spike train activity. *J. Neurosci. Methods* 105: 25-37.
- [27] Kass RE, Ventura VA (2001) A spike train probability model. *Neural Comput.* 13: 1713-1720.

- [28] Brown EN, Barbieri R, Eden UT, Frank LM (2003) Likelihood methods for neural data analysis. in *Computational Neuroscience: A comprehensive Approach*. (CRC Press, Boca Raton).
- [29] Chornoboy ES, Schramm LP, Karr AF (1988) Maximum likelihood identification of neural point process systems. *Biol. Cybern.* 59: 265-275.
- [30] Rieke F, Warland D, de Ruyter van Steveninck R, Bialek W (1997) *Spikes: Exploring the Neural Code*. MIT Press, Cambridge.
- [31] Borst A, Theunissen FE (1999) Information theory and neural coding. *Nat. Neurosci.* 2: 947-957.
- [32] Reich DS, Melcher F, Victor JD (2001) Independent and redundant information in nearby cortical neurons. *Science* 294: 2566-2568.
- [33] Nirenberg S, Carcieri SM, Jacobs AL, Latham PE (2001) Retinal ganglion cells act largely as independent encoders. *Nature* 411: 698-701.
- [34] Strong SP, Koberle R, de Ruyter van Steveninck RR, Bialek W (1998) Entropy and information in neural spike trains. *Phys. Rev. Lett.* 80: 197-200.
- [35] Berger T(2003) Living information theory. *IEEE Information Theory Society Newsletter* 53: 1-20.
- [36] Kandel ER, Schwartz JH, Jessell TM (2000) *Principles of Neural Science*. McGraw-Hill Publishing Co., Columbus.
- [37] Ferrier D (1886) *The functions of the brain (2nd. ed.)*. Smith, Elder, & Co., London.
- [38] Bianchi L (1922) *The mechanism of the brain and the function of the frontal lobes*. E. & S. Livingstone., Edinburgh.

- [39] Franz SI (1907) *On the functions of the cerebrum: The frontal lobes*. Science Press, New York.
- [40] Jacobsen CF (1936) Studies of cerebral function in primates: I. The functions of the frontal association areas in monkeys. *Comparative Psychology Monographs* 13: 1-60.
- [41] Hunter WS (1913) The delayed reaction in animals. *Behavioral Monographs* 2: 21-30.
- [42] Funahashi S, Bruce CJ, Goldman-Rakic PS (1989) Mnemonic coding of visual space in the monkeys dorsolateral prefrontal cortex. *J. Neurophysiol.* 61: 331-349.
- [43] Funahashi S, Bruce CJ, Goldman-Rakic PS (1990) Visuospatial coding in primate prefrontal neurons revealed by oculomotor paradigms. *J. Neurophysiol.* 63: 814-831.
- [44] Funahashi S, Bruce CJ, Goldman-Rakic PS (1991) Neuronal activity related to saccadic eye movements in the monkeys dorsolateral prefrontal cortex. *J. Neurophysiol.* 65: 1464-1483.
- [45] Funahashi S, Bruce CJ, Goldman-Rakic PS (1993) Dorsolateral prefrontal lesions and oculomotor delayed-response performance: Evidence for mnemonic scotomas. *J. Neurosci.* 13: 1479-1497.
- [46] Levy R, Goldman-Rakic PS (1999) Association of storage and processing functions in the dorsolateral prefrontal cortex of the nonhuman primate. *J. Neurosci.* 19: 5149-5158.
- [47] Levy R, Goldman-Rakic PS (2000) Segregation of working memory functions within the dorsolateral prefrontal cortex. *Exp. Brain Res.* 133: 23-32.

- [48] Ó Scalaidhe SP, Wilson FA, Goldman-Rakic PS (1999) Face-selective neurons during passive viewing and working memory performance of rhesus monkeys: Evidence for intrinsic specialization of neuronal coding. *Cereb. Cortex* 9: 459-475.
- [49] Wilson FA, Ó Scalaidhe SP, Goldman-Rakic PS (1993) Dissociation of object and spatial processing domains in primate prefrontal cortex. *Science* 260: 1955-1958.
- [50] Petrides M (2000) The role of the mid-dorsolateral prefrontal cortex in working memory. *Exp. Brain Res.* 133: 44-54.
- [51] Petrides M, Pandya DN (1994) Comparative architectonic analysis of the human and macaque frontal cortex. in *Handbook of neuropsychology* Vol. 9: 17-58 (Elsevier, Amsterdam).
- [52] Ungerleider LG, Mishkin M (1982) Two cortical visual system. in *Analysis of visual behavior* : 549-586 (MIT Press, Cambridge).
- [53] Bussey TJ, Wise SP, Murray EA (2001) The role of ventral and orbital prefrontal cortex in conditional visuomotor learning and strategy use in rhesus monkeys (*Macaca mulatta*). *Behavioral Neuroscience* 115: 971-982.
- [54] Gaffan D, Harrison S (1988) Inferotemporal-frontal disconnection and fornix transection in visuomotor conditional learning by monkeys. *Behav. Brain Res.* 31: 149-163.
- [55] Parker A, Gaffan D (1998) Memory after frontal/temporal disconnection in monkeys: Conditional and nonconditional tasks, unilateral and bilateral frontal lesions. *Neuropsychologia* 36: 259-271.



- [56] Wang M, Zhang H, Li BM (2000) Deficit in conditional visuomotor learning by local infusion of bicuculline into the ventral prefrontal cortex in monkeys. *European Journal of Neuroscience* 12: 3787-3796.
- [57] Murray EA, Bussey TJ, Wise SP (2000) Role of prefrontal cortex in a network for arbitrary visuomotor mapping. *Exp. Brain Res.* 133: 114-129.
- [58] Varela F, Lachaux JP, Rodriguez E, Martinerie J. (2001) The brainweb: phase synchronization and large-scale integration. *Nat. Rev. Neurosci.*, 2:229-239.
- [59] Abeles M (1982) *Local cortical circuits*. Springer, Berlin.
- [60] Paml G (1990) Cell assemblies as a guideline for brain research. *Concepts Neurosci.*, 1:133-147.
- [61] Eichenbaum H (1993) Thinking about brain cell assemblies. *Science*, 261:993-994.
- [62] Damasio A (1990) Synchronous activation in multiple cortical areas: a mechanism for recall. *Sem. Neurosci.*, 2:287-296.
- [63] Llinas R, Ribary U, Contreras D, Pedroarena C (1998) The neuronal basis for consciousness. *Phil. Trans. R. Soc. Lond. B*, 353:1841-1849.
- [64] Edelman G (1987) *Neural Darwinism*. Basic Books, New York.
- [65] Varela FJ (1995) Resonant cell assemblies: a new approach to cognitive functions and neuronal synchrony. *Biol. Res.*, 28:81-95.
- [66] Goldman-Rakic PS (1988) Topography of cognition: parallel distributed networks in primate association cortex. *Annu. Rev. Neurosci.*, 11:137-156.
- [67] Mesulam MM (1990) Large-scale neurocognitive networks and distributed processing for attention, language, and memory. *Ann. Neurol.*, 28:597-613.

- [68] Goldman-Rakic PS, Chafee M, Friedman H(1992) Prefrontal Cortex: Contribution to Memory and Cognition. in *Brain Mechanism of Perception and Memory: from Neuron to Behavior*. 445-456 (Oxford Univ. Press, New York).
- [69] Lee H, Simpson GV, Logothetis NK, Rainer G (2005) Phase locking of single neuron activity to theta oscillations during working memory in monkey extrastriate visual cortex. *Neuron*, 45:147-156.
- [70] Scherberger H, Jarvis MR, Andersen RA (2005) Cortical local field potential encodes movement intentions in the posterior parietal cortex. *Neuron*, 46:347-354.
- [71] Pesaran B, Pezaris JS, Sahani M, Mitra PP, Andersen RA (2002) Temporal structure in neuronal activity during working memory in macaque parietal cortex. *Nat. Neurosci.*, 5:805-811.
- [72] Percival DB and Walden AT (1993) *Spectral analysis for physical applications: multitaper and conventional univariate techniques*. Cambridge University Press, Cambridge.
- [73] Bour LJ, van Gisbergen JA, Bruijns J, Ottes FP (1984) The double magnetic induction method for measuring eye movement—results in monkey and man. *IEEE Trans. Biomed. Eng.*, 31(5):419-427.
- [74] Levitt JB, Lewis DA, Yoshioka T, Lund JS (1993) Topography of pyramidal neuron intrinsic connections in macaque monkey prefrontal cortex (area 9 and 46). *J. Comp. Neurol.*, 338(3):360-376.
- [75] Bradley E and Tibshirani RJ (1993) *An introduction to the bootstrap*. Chapman & Hall/CRC, London.

- [76] Pipa G (2006) *The neuronal code: Development of tools and hypotheses for understanding the role of synchronization of neuronal activity*. dissertation, TU Berlin.
- [77] Thomson DJ (1982) Spectrum estimation and harmonic analysis. *Proc. IEEE*, 70, 1055-1096.
- [78] G Pipa, DW Wheeler, W Singer, D Nikolic (2007) NeuroXidence: A Non-parametric Test on Excess or Deficiency of Joint-Spike Events. *J.Comput.Neurosci.*, PM:18219568, DOI 10.1007/s10827-007-0065-3.
- [79] G. Pipa, A. Riehle, S. Grün (2006) Validation of task-related excess of spike coincidences based on NeuroXidence. *Neurocomputing*, 70: 2064-2068.
- [80] Délage (1919) *Le rêve. étude psychologique, philosophique et littéraire*. Presses Universitaires de France, Paris.
- [81] Hebb DO (1949) *The organization of behavior*. Wiley, New York.
- [82] Singer W, Engel AK, Kreiter AK, Munk MH, Neuenschwander S, Roelfsema PR (1997) Neuronal assemblies: necessity, signature and detectability. *Trends in Cog. Sci.*, 1:252-261.
- [83] Fuster JM, Alexander GE (1971) Neuron activity related to short-term memory. *Science*, 173:652-654.
- [84] Goldman-Rakic PS (1995) Cellular basis of working memory. *Neuron*, 14:477-485.
- [85] Vaadia E, Haalman I, Abeles M, Bergman H, Prut Y, Slovin H, Aertsen A (1995) Dynamics of neuronal interactions in monkey cortex in relation to behavioural events. *Nature*, 373:515- 518.

- [86] Sakurai Y, Takahashi S (2006) Dynamic synchrony of firing in the monkey prefrontal cortex during working-memory tasks. *J. Neurosci.*, 26:10141-10153.

# Acknowledgement

First of all, I would like to thank Prof. Wolf Singer and Prof. Horst Stöcker. They give me this great opportunity to study in *Frankfurt International Graduate School for Science* (FIGSS) and continue my study in neuroscience field. Secondly, I would like to thank Dr. Gordon Pipa, my group leader, who led me into neuroscience field hand by hand. Because my background is physics and at first it was a hard time for me to step into neuroscience, he guided me with so much patience and encourage me a lot during my study. He is not only my mentor, but also my friend.

I am grateful to many friends: Dr. Diek Wheeler, Dr. Raul Muresan, Dr. Michael Wibral, Prof. Debin Huang, Prof. Nanhui Chen, Dr. Shan Yu and Leona Schild. We have a great time during my study in Frankfurt, not only in science, but also in everyday's life.

I would like to thank my collaborators Dr. Matthias Munk and Dr. Kerstin Schmit. I also appreciate support from Prof. Jochen Trisch from FIAS neuroscience group.

Last but most important, my family and my girlfriend, who support me and encourage me whenever I feel disappointment. Thank you father, mother, sister and Xuefei.

# Curriculum Vitae

**Wei Wu**

## Personal Data

Date of Birth January 16<sup>th</sup> 1979

City of Birth Hebei, China



## Education

2004-2008 PhD. Student, Frankfurt International Graduate School for Science (*FIGSS*), Frankfurt, Germany

2004 Master in Physics, Beijing Normal University, China

2001-2004 Graduate student in Physics Department, Beijing Normal University, China

2001 Bachelor in Physics, Beijing Normal University, China

1997-2001 Undergraduate student in Physics Department, Beijing Normal University, China

## **Publications**

Wei Wu, Diek W. Wheeler, Ellen S. Staedtler, Matthias H.J. Munk,

Gordon Pipa :

Behavioral performance modulates spike field coherence

in monkey prefrontal cortex, *NeuroReport*, 19(2): 235-238. 2008